AFRL-AFOSR-VA-TR-2022-0096

Combustion Mechanisms of HAN-based Green Monopropellants

Shafirovich, Evgeny
UNIVERSITY OF TEXAS AT EL PASO
500 W UNIVERSITY AVE
EL PASO, TX, 79968
USA

02/08/2022
Final Technical Report

Air Force Research Laboratory
Air Force Office of Scientific Research
Arlington, Virginia 22203
Air Force Materiel Command

REPORT DOCUMENTATION PAGE

PLEASE DO NOT RETURN YOUR FORM TO THE ABOVE ORGANIZATION.

1. REPORT DATE	**2. REPORT TYPE**	**3. DATES COVERED**	
20220208	Final	**START DATE** 20180615	**END DATE** 20220115

4. TITLE AND SUBTITLE
Combustion Mechanisms of HAN-based Green Monopropellants

5a. CONTRACT NUMBER	**5b. GRANT NUMBER** FA9550-18-1-0406	**5c. PROGRAM ELEMENT NUMBER** 61102F
5d. PROJECT NUMBER	**5e. TASK NUMBER**	**5f. WORK UNIT NUMBER**

6. AUTHOR(S)
Evgeny Shafirovich

7. PERFORMING ORGANIZATION NAME(S) AND ADDRESS(ES)
UNIVERSITY OF TEXAS AT EL PASO
500 W UNIVERSITY AVE
EL PASO, TX 79968
USA

8. PERFORMING ORGANIZATION REPORT NUMBER

9. SPONSORING/MONITORING AGENCY NAME(S) AND ADDRESS(ES)	**10. SPONSOR/MONITOR'S ACRONYM(S)**	**11. SPONSOR/MONITOR'S REPORT NUMBER(S)**
Air Force Office of Scientific Research 875 N. Randolph St. Room 3112 Arlington, VA 22203	AFRL/AFOSR RTA1	AFRL-AFOSR-VA-TR-2022-0096

12. DISTRIBUTION/AVAILABILITY STATEMENT
A Distribution Unlimited: PB Public Release

13. SUPPLEMENTARY NOTES

14. ABSTRACT
Monopropellants based on hydroxylammonium nitrate (HAN) are a low-toxic, highperformance alternative to hydrazine in space propulsion systems. However, their combustion
and the decomposition of energetic ionic liquids used in their formulations, such as HAN and 2-hydroxyethylhydrazinium nitrate (HEHN), are not well understood. In addition, gelling such propellants may provide long-term stability of compositions with energetic and catalytic particles, but the effect of gelling on the combustion characteristics and mechanisms of HANbased propellants is unclear. The present work included thermoanalytical studies on HAN and
HEHN decomposition as well as strand burner experiments with aqueous HAN/methanol propellants. The thermoanalytical studies involved thermogravimetric analysis (TGA), differential scanning calorimetry (DSC), mass spectroscopy, and Fourier transform infrared spectroscopy. It has been shown that the decomposition of HEHN has two stages. The apparent activation energies are 113.7 ± 1.7 kJ/mol at the first stage and 123.6 ± 2.5 kJ/mol at the second stage. The thermal decomposition temperature of HAN decreased by about 50 ºC with increasing pressure to 2 MPa, but remained virtually constant with further increasing pressure, apparently because of suppressed evaporation of nitric acid. In the strand burner experiments with HAN/methanol/water propellants, different pressure dependencies of the linear burning rate were determined over the pressure range of 9 – 30 MPa.

15. SUBJECT TERMS

16. SECURITY CLASSIFICATION OF:			**17. LIMITATION OF ABSTRACT**	**18. NUMBER OF PAGES**
a. REPORT	**b. ABSTRACT**	**c. THIS PAGE**		
U	U	U	UU	47

19a. NAME OF RESPONSIBLE PERSON	**19b. PHONE NUMBER** *(Include area code)*
MITAT BIRKAN	426-7234

Final Performance Report

Combustion Mechanisms of HAN-based Green Monopropellants

Federal Grant Number:	FA9550-18-1-0406
Grant Period:	6/15/2018 – 1/15/2022
Reported Period:	6/15/2018 – 1/15/2022
Prepared for:	Air Force Office of Scientific Research Space Propulsion and Power Program Dr. Mitat A. Birkan

Submitted by: Evgeny Shafirovich, Principal Investigator
Department of Aerospace and Mechanical Engineering
The University of Texas at El Paso

Abstract

Monopropellants based on hydroxylammonium nitrate (HAN) are a low-toxic, high-performance alternative to hydrazine in space propulsion systems. However, their combustion and the decomposition of energetic ionic liquids used in their formulations, such as HAN and 2-hydroxyethylhydrazinium nitrate (HEHN), are not well understood. In addition, gelling such propellants may provide long-term stability of compositions with energetic and catalytic particles, but the effect of gelling on the combustion characteristics and mechanisms of HAN-based propellants is unclear. The present work included thermoanalytical studies on HAN and HEHN decomposition as well as strand burner experiments with aqueous HAN/methanol propellants. The thermoanalytical studies involved thermogravimetric analysis (TGA), differential scanning calorimetry (DSC), mass spectroscopy, and Fourier transform infrared spectroscopy. It has been shown that the decomposition of HEHN has two stages. The apparent activation energies are 113.7 ± 1.7 kJ/mol at the first stage and 123.6 ± 2.5 kJ/mol at the second stage. The thermal decomposition temperature of HAN decreased by about 50 ºC with increasing pressure to 2 MPa, but remained virtually constant with further increasing pressure, apparently because of suppressed evaporation of nitric acid. In the strand burner experiments with HAN/methanol/water propellants, different pressure dependencies of the linear burning rate were determined over the pressure range of 9 – 30 MPa. An increase in the burning rate by over 50% was observed at 12 – 14 MPa and explained by supercritical fluid effects. Gelling the propellant with 1 wt% polyacrylamide in an acoustic mixer suppressed these variations, leading to a consistent pressure exponent of 1.15 ± 0.05 over the pressure range of 4 – 30 MPa. Thermoanalytical studies have shown that the effect of gelling on the combustion of HAN/methanol/water propellants is hydrodynamic in nature.

Contents

1. Two-stage Decomposition of 2−Hydroxyethylhydrazinium Nitrate (HEHN)

1.1. Introduction

Hydrazine has been extensively used as a monopropellant in the space industry. However, its high toxicity and vapor pressure lead to high handling costs. For this reason, there is a growing interest in replacing hydrazine with the so-called green monopropellants, which usually include a fuel and an oxidizer, dissolved in water [1–5]. One promising fuel for these applications is the hydrazine-derived ionic liquid 2-hydroxyethylhydrazinium nitrate (HEHN, $[HO\text{-}CH_2\text{-}CH_2\text{-}NH_2\text{-}NH_2^+][NO_3^-]$), which has a high solubility in water, a low vapor pressure, and low toxicity [6]. HEHN is formed by the reaction between hydroxyethylhydrazine (HEH, $HO\text{-}CH_2\text{-}CH_2\text{-}NH\text{-}NH_2$) and HNO_3 [7]. Recently, it has been proposed to also use HEHN as an additive to unsymmetrical dimethylhydrazine (UDMH, a hypergolic rocket fuel) [8] and as a substitute for the Otto fuel II monopropellant in propulsion systems of torpedoes [9]. Unfortunately, the available data on the decomposition of HEHN are scarce.

Alfano et al. [10] studied laser ignition of hydroxylammonium nitrate/HEHN mixtures and reported that experiments with HEHN alone were uneventful. Differential scanning calorimetry conducted by Shamshina et al. [11] has revealed that thermal decomposition of HEHN starts at 193 ºC. They also conducted drop tests with several catalysts at temperatures from 50 to 200 ºC. Catalytic ignition of HEHN, with a visible flame, was observed with Shell 405 at 150 °C, while other tested catalysts did not show any activity.

Chowdhury and Thynell [12] studied HEHN decomposition using confined rapid thermolysis, where a 0.5 μL sample was heated at a heating rate of 2000 K/s to a temperature of 270, 280, or 290 °C. The evolved gases were detected with a Fourier transform infrared (FTIR) spectrometer and a time-of-flight mass spectrometer. The decomposition products were H_2O, N_2O, N_2, and NH_3, with minor quantities of NO and CO_2. Based on their experimental results, they have proposed a three-step reaction scheme, where the first step corresponds to the proton transfer to form HEH and HNO_3, the second step is an autocatalytic reaction of HEHN with HNO_3, and the third step is a global reaction between HEH and HNO_3. Table 1-1 shows the estimated effective activation energy and pre-exponential factor for these reactions.

Table 1-1. Reaction steps and their kinetic parameters in the decomposition of HEHN [12].

Step	Reaction	Activation energy	Pre-exponential factor
1	$HEHN \rightarrow HEH + HNO_3$	183.0 kJ·mol^{-1}	2.0×10^{16} s^{-1}
2	$HEHN + HNO_3 \rightarrow HEH + 2\ HNO_3$	124.8 kJ·mol^{-1}	3.9×10^{12} mol^{-1}·cm^3·s^{-1}
3	$HEH + HNO_3 \rightarrow 2.5\ H_2O + 0.42\ N_2O + 1.08\ N_2 + 0.042\ O_2 + CH_3CHO$	24.3 kJ·mol^{-1}	8.3×10^5 mol^{-1}·cm^3·s^{-1}

More recently, Swami et al. [9] studied the thermal decomposition of HEHN using thermogravimetric analysis (TGA) and FTIR spectroscopy. At a heating rate of 10 K/min, two distinct periods of mass loss were observed. First, the mass decreased by 10% in the temperature range of 40 – 80 °C, which was attributed to the evaporation of water absorbed by the sample. Next, the mass dropped by 75% between 180 °C and 240 °C because of HEHN decomposition. The identified product gases were N_2O, CO_2, NH_3, HNO_3, and NO_2.

To better understand the kinetics and mechanism of HEHN decomposition, more research is needed. The objective of the present work was to investigate the kinetics of thermal decomposition of HEHN by thermoanalytical methods and to identify the evolved gas products using mass spectrometry and FTIR spectroscopy.

1.2. Experimental

HEHN was synthesized by careful addition of HNO_3 to HEH under controlled conditions in glass or Teflon as described in reference [7]. Special care was taken to use the highest purity reagents and minimize any contamination in the synthesis. Gas chromatography has shown that its purity is at least 97%.

The decomposition was studied using a thermogravimetric analyzer (Netzsch TG 209 F1 Iris) and a differential scanning calorimeter (Netzsch DSC 404 F1 Pegasus). In both TGA and DSC tests, a 10 mg sample of HEHN was placed, using a pipette, into an alumina crucible and heated in a 20 mL/min helium flow at different heating rates over the range from 1 to 10 °C/min. Three vacuum cycles were performed to purge residual air and to evaporate any water that could be absorbed by the sample during storage.

In the DSC work, temperature and sensitivity calibrations were performed to accurately determine the peak temperatures. In the TGA work, the balance was also calibrated. Correction runs for the crucibles were performed before each DSC or TGA test. The TGA and DSC runs were repeated eight times to ensure reproducibility.

The evolved gases were identified with a quadrupole mass spectrometer (Netzsch QMS 403D Aëolos) and a Fourier-transform infrared spectrometer (Bruker Tensor II). Each instrument was connected to the TGA via a transfer line. To avoid condensation of water, the transfer line of the mass spectrometer was heated to 150 ºC, and that of the FTIR spectrometer was heated 200 ºC. The electron impact ionization energy was set to 25 eV in the mass spectrometer, at a speed of 200 ms for each mass unit, while the FTIR spectrometer measured spectrum every 625 ms with a resolution of 4 cm^{-1}.

1.3. Results

1.3.1. Thermoanalytical experiments

In the TGA and DSC runs, the maximum temperature was 400 °C. HEHN was decomposed and a black, flaky solid residue was observed in the crucible after the run. The crucibles were fully cleaned by heating up to 1000 °C.

Figure 1-1 shows the typical TG curves at heating rates of 1, 2.5, 5, and 10 °C/min. In contrast with the work in reference [9], no mass loss due to evaporation of water was detected in our experiments, which is explained by the high purity of the tested HEHN and by conducting vacuum cycles before the run. It is seen that the TG curves have two distinct mass loss regimes at temperatures higher than the boiling point of water. The first regime, where the mass decreases by approximately 45%, is observed over the temperature range of 140 – 180 ºC at a heating rate of 1 °C/min. With increasing the heating rate to 10 °C/min, the end temperature of this regime increases to 220 ºC. The second regime, characterized by 45 – 80% mass loss, occurs over the temperature range of 180 – 210 ºC at a heating rate of 1 °C/min and 220 – 250 ºC at 10 °C/min. The existence of two mass loss regimes implies that there are two stages in the decomposition of HEHN. In the TGA trace in reference [9], the mass decreases smoothly with increasing temperature and the differential thermogravimetric analysis showed only a single peak for the decomposition. It should be noted that purity of the tested HEHN was not reported in reference [9].

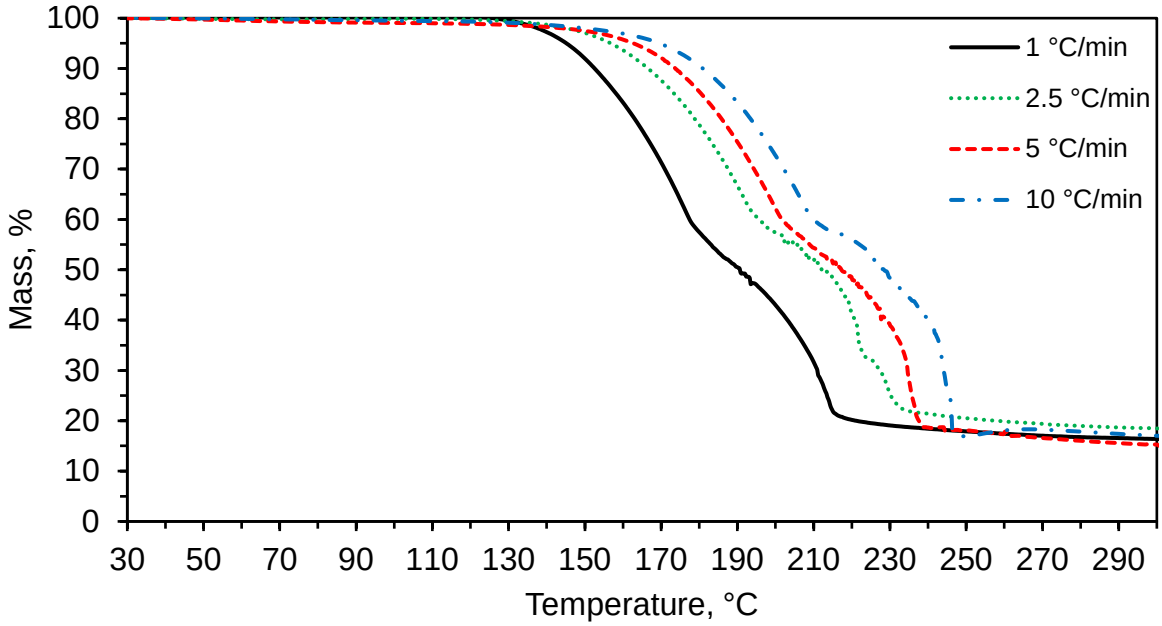

Fig. 1-1. TGA curves of HEHN decomposition at different heating rates.

Figure 1-2 shows the typical HEHN DSC curves at 1, 2.5, 5, and 10 °C/min. It is seen that each curve has two evident exothermic peaks about 50 ºC apart. At a heating rate of 1 °C/min, the peaks are at 165 ºC and 210 ºC. With increasing the heating rate, the peak temperatures increase, reaching 196 ºC and 244 ºC at 10 °C/min. In each curve, the second peak is higher and sharper than the first one.

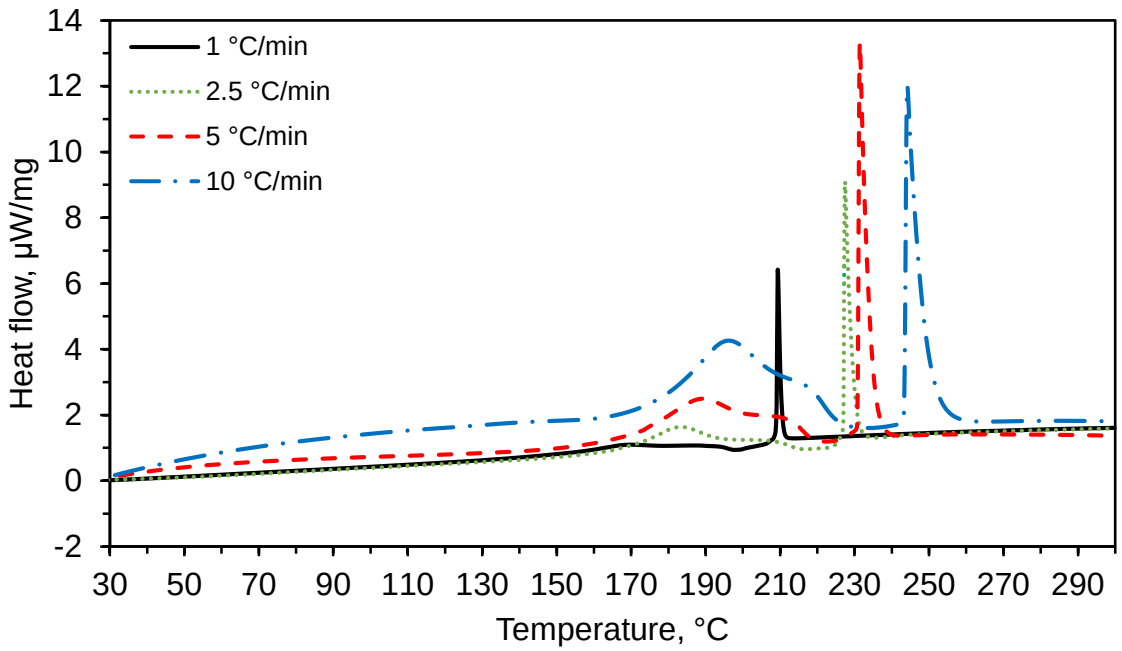

Fig. 1-2. DSC curves of HEHN decomposition at heating rates of 1, 2.5, 5, and 10 °C/min

The existence of two exothermic peaks correlates with the two regimes of mass loss observed in the TGA. Figure 1-3 shows that the temperature of the first DSC peak correlates with the first mass loss regime in the TG curves, while the second peak corresponds to the final, drastic loss of mass.

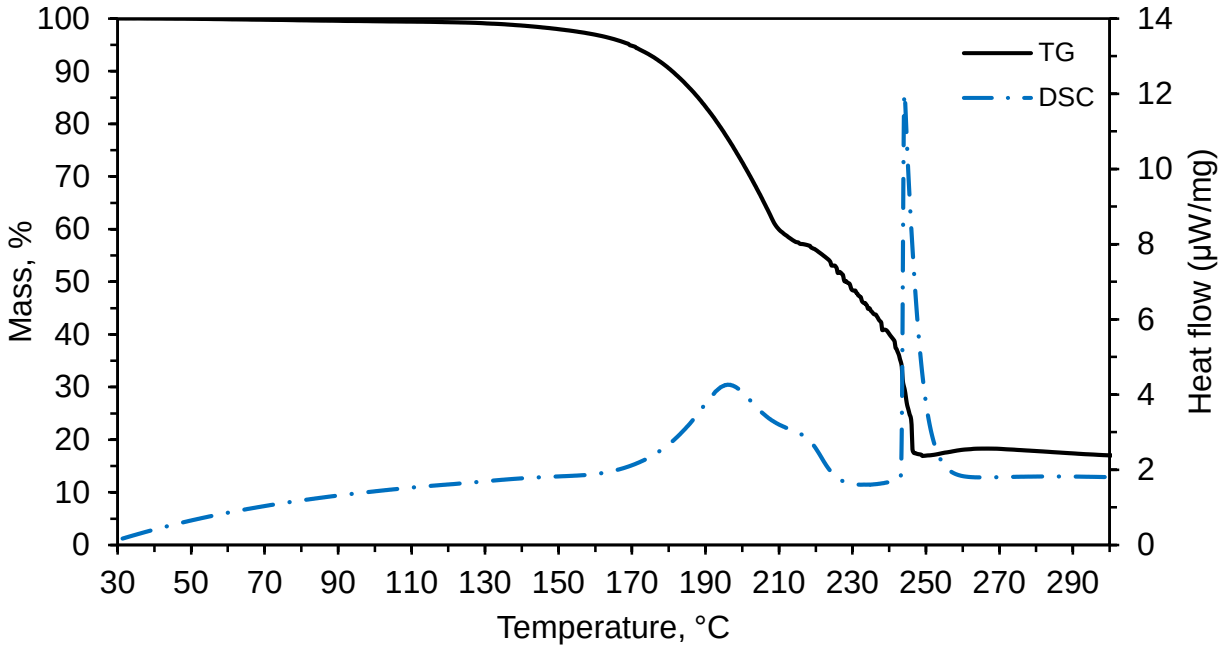

Fig. 1-3. TG and DSC curves of HEHN decomposition at 10 °C/min.

1.3.2. Determination of the kinetic parameters

The obtained TGA and DSC data were analyzed using Netzsch Thermokinetics 3.1 software with the goal of extracting kinetic information via model-free analysis (based on Ozawa-Wall-Flynn [13–16] and Kissinger [17–19] methods) and, as the next step, model-based analysis. Table 1-2 shows the obtained values for the activation energy and pre-exponential factor for both stages of the decomposition.

Table 1-2. Kinetic parameters of HEHN decomposition obtained by the Ozawa-Wall-Flynn (TGA – OWF and DSC – OWF), and Kissinger (DSC − K) methods.

Stage	**Activation energy**	**Pre-exponential factor**
	kJ·mol^{-1}	**s^{-1}**
	TGA – OWF	
1	97.6 ± 7.8	1.6×10^{8}
2	87 – 119	$7.8 \times 10^{6} – 1.7 \times 10^{10}$
	DSC – OWF	
1	145.2 ± 0.9	4.1×10^{17}
2	155.2 ± 9.0	2.2×10^{17}
	DSC – K	
1	143.6 ± 0.3	2.9×10^{17}
2	217.9 ± 1.7	6.0×10^{23}

It is worth noting that the Kissinger and Ozawa-Wall-Flynn analyses of the DSC data have produced virtually the same activation energy of the first stage, 144 – 145 kJ/mol. However, the value determined based on the TGA data is lower by about 50 kJ/mol. Additionally, there is a large difference between the values of the activation energy of the second stage extracted by two methods from the same DSC data. These discrepancies indicate that the model-free methods involve assumptions that may be invalid for the investigated reactions. Furthermore, the Kissinger method does not allow determination of the reaction order. Model-based methods do not involve

such assumptions/limitations and can provide more detailed information on the reaction mechanism.

The model-based analysis was conducted to determine the decomposition models that fit the TGA data. Since two stages of HEHN decomposition were observed, the models with two consecutive reactions were tested. The analysis was performed based on seven kinetic models (Table 1-3) for each of the two stages, totaling 49 two-stage decomposition models. The model abbreviations in Table 3 are commonly used in the literature. Also, as usual, *f(e,p)* is a function of conversion degree α ($\alpha = p = 1 - e$), K_{cat} is the catalytic constant, and X is the concentration of the autocatalyst (e.g., HNO_3 in the scheme shown in Table 1-1).

Table 1-3. Kinetic models tested for fitting the TGA data on decomposition of HEHN.

Model abbreviation	***f(e,p)***	**Reaction type**
F1	e	First order
F2	e^2	Second order
F*n*	e^n	n^{th} order
B1	ep	Autocatalysis via the first order Prout-Tompkins equation
B*na*	$e^n p^a$	Autocatalysis via the n^{th} order Prout-Tompkins equation
C1-X	$e(1 + K_{cat}X)$	First order autocatalysis
C*n*-X	$e^n(1 + K_{cat}X)$	n^{th} order autocatalysis

It should be noted that the Thermokinetics software also includes the Avrami-Erofeev equations (kinetic models A2, A3, and A*n*), which describe sigmoid-type kinetic curves similar to those obtained in autocatalysis. However, these equations describe processes with nucleation and growth, such as crystallization, and they should not be used for autocatalytic processes, where branching is an inherent part of the reaction mechanism [21]. For this reason, the Avrami-Erofeev equations were not tested in the model-based analysis of HEHN decomposition.

For a successful analysis, the Thermokinetics software relies on realistic initial conditions; thus they were based on the kinetic parameters obtained by model-free analysis (TGA-OWF, DSC-OWF, and DSC-K methods) shown in Table 2. In the TGA-OWF case, the kinetic parameters of the second stage could not be reliably determined. However, to provide the initial conditions for

model-based analysis, the parameters calculated at 0.55 conversion degree, i.e. at the beginning of the second stage (see Fig. S5), were used. The software carries out a nonlinear regression calculation using the Prince-Dormand method to solve 5th-degree ordinary differential equations. The quality of fit is determined by performing Fisher's exact test (F-test), where the algorithm searches for the model with the least variance [20]. This model is characterized by F_{exp} value being equal to unity, while others get larger values of F_{exp}.

First, the analysis determined the best two-stage reaction models for each of the three initial conditions. For TGA-OWF, DSC-OWF, and DSC-K initial conditions, two, two, and one models, respectively, are characterized by F_{exp} = 1.00. Next, the software compared these models between each other and determined their F_{exp} values in this group of five, which were in the range from 1.00 to 1.02. Table 1-4 presents these models and the obtained kinetic parameters.

Table 1-4. Kinetic parameters determined in model-based analysis of the TGA data on HEHN decomposition.

Initial conditions	**First stage**				**Second stage**				F_{exp}
	Model	**E**	**A**	**n**	**Model**	**E**	**A**	n	
		kJ·mol^{-1}	**M^{1-n}·s^{-1}**			**kJ·mol^{-1}**	**M^{1-n}·s^{-1}**		
TGA-OWF	B*na*	111.9	1.5×10^9	2.31	C1-X	127.3	2.0×10^{10}	1	1.00
TGA-OWF	B*na*	112.5	1.6×10^9	2.28	C*n*-X	125.7	2.6×10^{10}	0.78	1.00
DSC-OWF	B*na*	115.8	4.2×10^9	2.26	C*n*-X	121.3	5.1×10^{10}	0.3	1.02
DSC-OWF	C*n*-X	112.6	4.1×10^8	2.57	F*n*	122.4	1.0×10^{11}	0.09	1.02
DSC-K	B*na*	115.8	4.2×10^9	2.26	F*n*	121.3	6.4×10^{10}	0.3	1.02

It should be noted that Thermokinetics software uses kinetic functions based on the conversion degree (see Table 1-3), where pre-exponential factors have a dimension of s^{-1} independently on the reaction order. To obtain the pre-exponential factors for kinetic functions based on concentrations, shown in Table 1-4, the molarity of HEHN was determined based on its density at 298 K, 1.428 g/cm^3.

Analysis of the five models in Table 1-4 shows a high confidence level for the first stage. Four models indicate that this stage is Prout-Tompkins autocatalysis (B*na*) with an activation energy of

112 – 116 kJ/mol and reaction order of 2.3. One model shows n^{th} order autocatalysis (C*n*-X) with the same activation energy and slightly different reaction order, 2.6. The results for the second stage show larger differences between the obtained models. Three of them show autocatalysis (C*n*-X) with a reaction order from 0.3 to 1, and two others show an n^{th} order reaction (F*n*) with a reaction order from 0.1 to 0.3. These discrepancies are not surprising, given the larger scatter for the second stage in the experimental TGA and DSC data. The activation energies of the second stage, obtained in the five models, are close to each other, 121 – 127 kJ/mol. The fractional order of the reaction indicates that the reaction mechanism is more complex than in the tested kinetic models.

Although these results do not allow one to make unambiguous conclusions on the precise kinetic model at each stage, several important features can be noted. The expected autocatalytic behavior was undoubtedly confirmed for the first stage. The average value and the standard deviation were determined for each stage of the five models. The obtained values of the apparent activation energy are: 113.7 ± 1.7 kJ/mol for the first stage and 123.6 ± 2.5 kJ/mol for the second stage. It is worth noting that the second stage has a higher apparent activation energy than the first one. Also, the second stage has a lower apparent reaction order.

1.3.3. Evolved gas analysis

During the thermal decomposition of HEHN, 38 m/z values were detected by mass spectrometry. Figure 1-4 shows the most intense MS signals generated during heating HEHN at a rate of 10 °C/min. Other signals were by 1 – 3 orders of magnitude less (ion currents of the order of 10^{-12} – 10^{-10} A), and many of them were possibly caused by fragmentation of HEH^+. Two stages of gas evolution are clearly seen in Fig. 1-4. The gases, identified using the literature data [22], include H_2O (m/z = 18), NH_3 (m/z = 16, 17), N_2 (m/z = 28), and NO (m/z = 30). The m/z = 44 curve could be produced by both N_2O and CO_2.

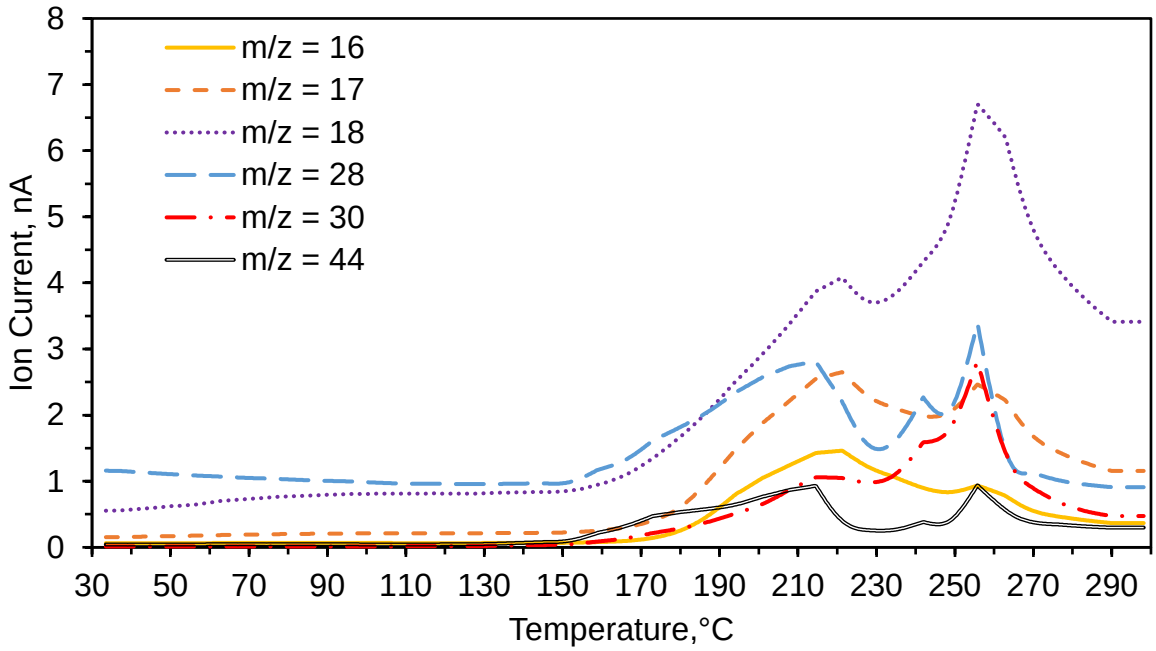

Fig. 1-4. Temperature profiles of the most intense lines in the mass spectra of gases evolved during TGA of HEHN at a heating rate of 10 °C/min. The measured ion current provides a relative measurement of the concentration of the stable species arriving in the ionization zone of the mass spectrometer.

Figure 1-5 shows some of the most intense FTIR signals generated during heating HEHN at a rate of 10 °C/min. The two stages are again seen clearly. In addition, Figure 1-6 shows the FTIR spectra obtained at temperatures of 196 °C and 251 °C (for clarity, in the range of wavelengths 700 – 2300 cm^{-1} with the most intense lines). The FTIR analysis confirms that a significant amount of NH_3 was released at both stages. It also clarifies that the m/z = 44 signal during the first stage was generated by N_2O and not by CO_2, while during the second stage the m/z = 44 signal was produced mainly by CO_2 and, to a lesser extent, by N_2O. It also shows intense lines of HNO_3 during the second stage. It should be noted that the FTIR plots show higher peak temperatures than in the MS temperature profiles. This difference is related to the fact that it takes different lengths of time for the evolved gas to get through the different transfer lines. An offset of ~10 °C is small and considered typically normal for a heating rate of 10 °C/min used in our instrumental arrangement.

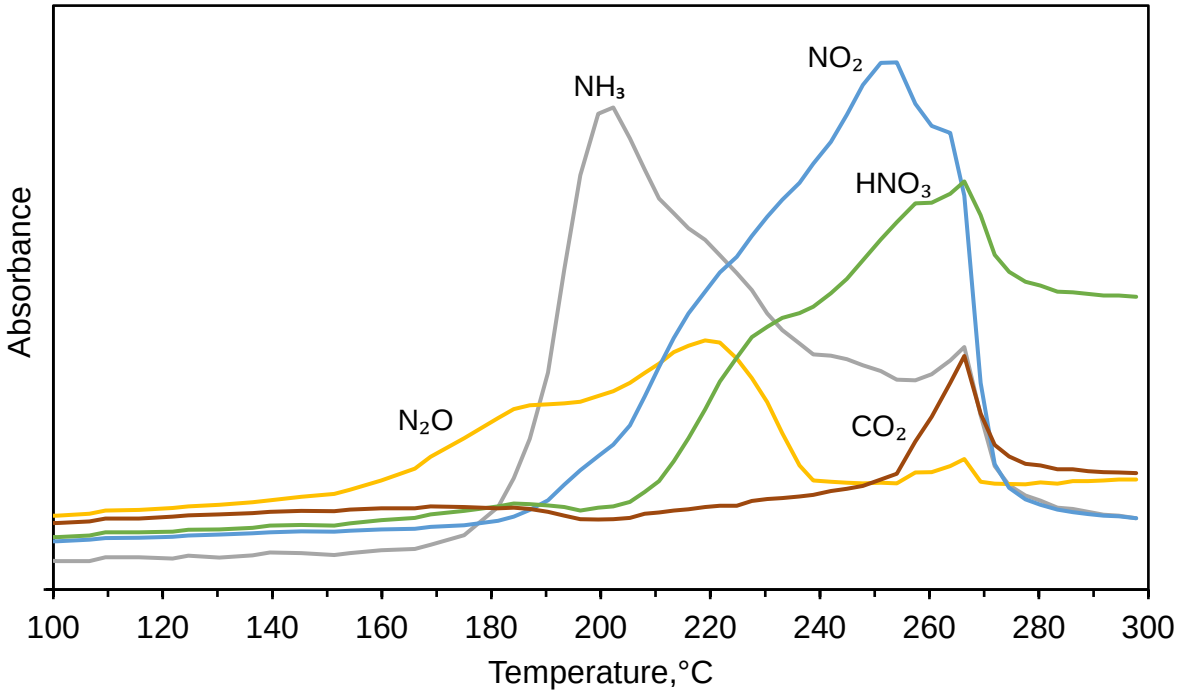

Fig. 1-5. Temperature profiles of the most intense lines in the FTIR spectra of gases evolved during TGA of HEHN at a heating rate of 10 °C/min.

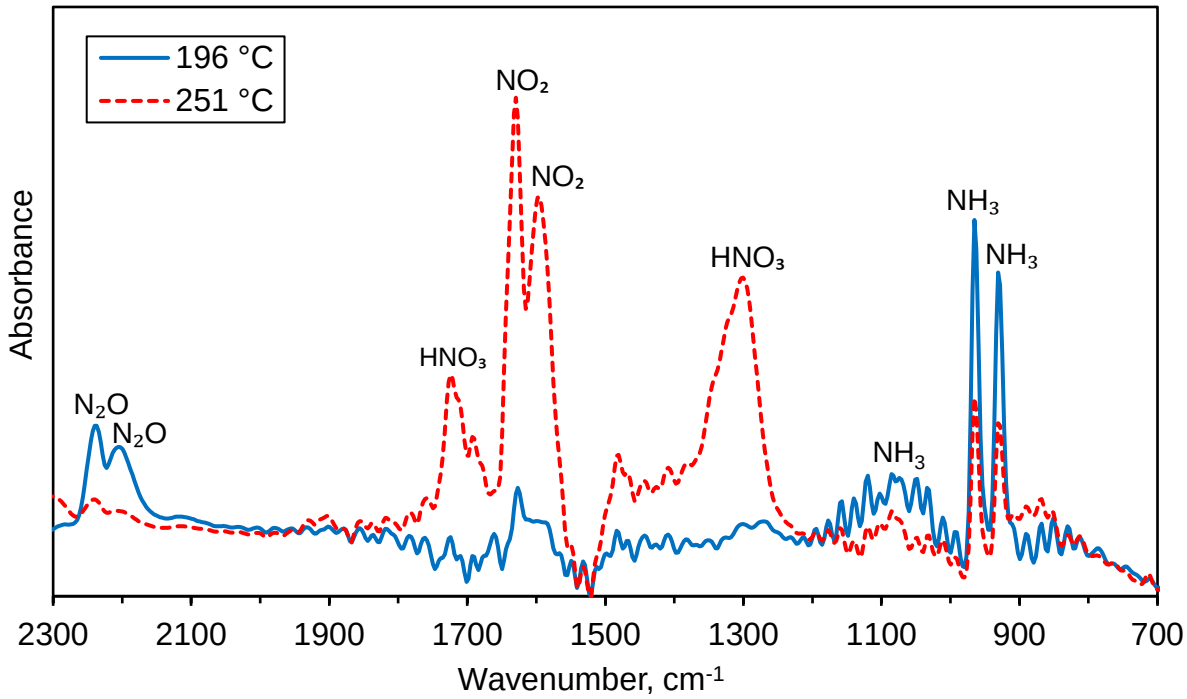

Fig. 1-6. FTIR spectra of gases evolved at 196 °C and 251 °C during TGA of HEHN at a heating rate of 10 °C/min.

1.4. Discussion

All the used techniques (TGA, DSC, MS, and FTIR spectroscopy) have clearly shown the existence of two stages of HEHN thermal decomposition. The apparent activation energies determined by the model-based thermal analysis, 113.7 ± 1.7 kJ/mol for the first stage and 123.6 ± 2.5 kJ/mol for the second stage, are relatively close, especially the latter, to the value of 124.8 kJ/mol obtained by Chowdhury and Thynell [12] for step 2 in their reaction mechanism (autocatalytic reaction between HEHN and HNO_3) and much lower than 183 kJ/mol for step 1 (proton transfer) in that mechanism (see Table 1-1). Apparently, the proton transfer reaction, despite its high activation energy, is able to produce a small initial number of HNO_3 molecules, the number of which is then dramatically increased by the autocatalytic reaction.

It should be noted that two phases of decomposition could not be observed in work [12], where the sample was heated to 270 – 290 °C at a heating rate of 2000 K/s (i.e. for 0.12 – 0.13 s), and the decomposition was occurring after that at a constant temperature.

The FTIR spectroscopy has shown a clear difference in the compositions of gases evolved during the two stages. At the first stage, NH_3 generates the most intense signal, followed by N_2O, whereas at the second stage NO_2 and HNO_3 prevail. The results of mass spectrometry complement the FTIR data. They show significant amounts of N_2 and NO. Note the symmetrical diatomic molecules of N_2 cannot be detected by FTIR spectroscopy.

Combining the results of MS and FTIR spectroscopy, one can suggest that the first stage of HEHN decomposition generates H_2O, N_2, NH_3, NO, N_2O, and NO_2. The composition of gases evolved during the second stage is different. Although it includes the same six gases, the amounts of NH_3 and N_2O significantly decreased, and strong signals of HNO_3 and CO_2 appeared. Note that the gases detected in [9] included NO_2, NH_3, N_2O, HNO_3, and CO_2, but they evolved via a single decomposition process.

These results imply that the reaction mechanism of HEHN decomposition differs from that proposed by Chowdhury and Thynell [12]. In particular, the reaction step 3 (see Table 1-1) should include NH_3, NO, NO_2, and CO_2. It should also be noted that the obtained FTIR spectra do not confirm the presence of acetaldehyde (CH_3CHO) postulated in that reaction mechanism. Further, the reaction mechanisms of the two stages, discovered in the present work, differ from each other.

To our knowledge, the existence of two stages of HEHN decomposition during linear heating has not been reported previously. The low-temperature stage of the mass loss in TGA experiments [9] was caused by the evaporation of water and not by decomposition of HEHN. No mass loss was observed at such temperatures in the present work, where a high-purity HEHN was tested and vacuum cycles were used to vaporize any absorbed water.

The interruption of decomposition at the end of the first stage and its restart at a higher temperature could be explained by the following scenario. Let us assume that the decomposition of HEHN produces active reactants and, in parallel, some condensed (liquid or solid) byproduct. The active reactants react between each other to produce gases. Let us then assume that the condensed byproduct can also decompose, but the activation energy of its decomposition is high.

In this case, at lower temperatures the decomposition of HEHN will lead to accumulation of the condensed byproduct in the sample, which will dilute the active reactants and decelerate their reaction. Increasing the temperature will promote the highly activated decomposition of the byproduct, which will also eliminate its hindering effect on the reaction between the active reactants.

The proposed scenario correlates with the observations of the higher apparent activation energy at the second stage. Further, the observed effect of the conversion degree on the kinetic parameters at the second stage in the Ozawa-Wall-Flynn analysis indicates a more complicated reaction mechanism during this stage, which accords with the hypothesis of a parallel decomposition reaction of the byproduct. Finally, the addition of one more reaction step (the decomposition of the byproduct) at the second stage may explain the observed difference between the compositions of evolved gases at the two stages of HEHN decomposition.

The TGA curves clearly show that some mass always remained in the crucible (as mentioned above, a black, flaky solid residue was observed), which indicates that the formation of some condensed byproduct did occur. Proposed formation of byproducts may be confirmed in the future by interrupting the TGA decomposition process to recover the material in the crucible for analysis.

Let us discuss what compound could be the proposed byproduct. In a prior experimental study [23], thermal decomposition of HEH occurred at about 215 °C and led to the formation of monomethylhydrazine and several other species, such as ethanolamine ($HOCH_2CH_2NH_2$, C_2H_7NO), ammonia, and hydrazine. In the present work, the decomposition of HEH could also occur at the surface of the crucible. This could lead to the formation of ethanolamine and ammonia through a series of heterogeneous reactions as follows:

$$HOCH_2CH_2NHNH_2 + \text{surface} \rightarrow HOCH_2CH_2NNH_{2(ad)} + H_{(ad)} \quad (1\text{-}1)$$

$$HOCH_2CH_2NHNH_2 + \text{surface} \rightarrow HOCH_2CH_2NH_{(ad)} + NH_{2(ad)} \quad (1\text{-}2)$$

$$HOCH_2CH_2NH_{(ad)} + H_{(ad)} \rightarrow HOCH_2CH_2NH_2 \quad (1\text{-}3)$$

$$NH_{2(ad)} + H_{(ad)} \rightarrow NH_3 \quad (1\text{-}4)$$

where the subscript (*ad*) indicates adsorbed species.

Since the boiling point of ethanolamine at 1 atm is 170 °C, it should form in the gaseous state during decomposition of HEHN and, hence, it cannot serve as the proposed condensed byproduct. Note that the species with m/z = 61, which corresponds to C_2H_7NO, was, indeed, detected during both stages of HEHN decomposition, but the signal was much smaller than for m/z = 17 (see Fig. 1-4).

Alternatively, the great evolution of ammonia at the first stage of HEHN decomposition implies that the decomposition of HEH may follow the following simple equation:

$$HOCH_2CH_2NHNH_2 \rightarrow C_2H_5NO + NH_3 \quad (1\text{-}5)$$

Five different C_2H_5NO structures are known in the literature, and the standard enthalpy of formation is reported for two of them, viz., acetamide and acetaldoxime: −315.6 kJ/mol and −85.8

kJ/mol, respectively (both in the solid state) [22]. Since the standard enthalpies of formation for HEH (liquid) and NH_3 (gas) are −203.4 kJ/mol [24] and −45.9 kJ/mol [22], respectively, the enthalpy of reaction Eq. (1-5) is equal to −158.1 kJ/mol if acetamide forms and +71.7 kJ/mol if acetaldoxime forms. Since the decomposition of HEH is exothermic, acetamide is a possible byproduct.

A bimolecular reaction of HEH decomposition could also produce a condensed compound and ammonia:

$$2\ HOCH_2CH_2NHNH_2 \rightarrow C_4H_{10}N_2O_2 + 2\ NH_3 \quad (1\text{-}6)$$

Seven different $C_4H_{10}N_2O_2$ structures are known in the literature, and the standard enthalpy of formation is reported for one of them, viz., ethanamine, N-ethyl-N-nitro-: −106.0 kJ/mol (in the liquid state) [22]. If this compound were to form, the enthalpy of reaction Eq. (1-6) would have been equal to +190.4 kJ/mol, which indicates that this reaction does not occur in our case. However, there are six other structures of $C_4H_{10}N_2O_2$ with unknown enthalpies of formation.

Further studies are needed to clarify the decomposition mechanism of HEHN and verify the proposed hypothesis.

1.5. Conclusions

Thermal decomposition of high-purity HEHN was studied using thermogravimetric analysis and differential scanning calorimetry. The decomposition is characterized by two regimes of mass loss in TGA and two distinct exothermic peaks in DSC, which indicates the existence of two stages in the overall decomposition process.

The effective kinetic parameters of both stages were determined using the Ozawa-Wall-Flynn, Kissinger, and model-based methods. The model-based analysis has shown autocatalytic behavior of the involved reactions and produced apparent activation energies of 113.7 ± 1.7 kJ/mol at the first stage and 123.6 ± 2.5 kJ/mol at the second stage, close to the value of 124.8 kJ/mol, previously obtained [12] for the autocatalytic reaction between HEHN and HNO_3.

Mass spectrometry and FTIR spectroscopy of gases evolved at different temperatures during TGA of HEHN confirm the existence of these two stages. The first stage generates H_2O, N_2, NH_3, NO, N_2O, and NO_2. The second stage also generates these gases (with smaller amounts of NH_3 and N_2O) plus HNO_3 and CO_2. These results show that the previously proposed [12] reaction mechanism of HEHN decomposition has to be expanded to include NH_3, NO, NO_2, and CO_2 gas products.

The observed existence of two stages in the thermal decomposition of HEHN could be explained by the formation of a condensed byproduct, which, in turn, decomposes via a highly activated reaction.

1.6. References

[1] R.L. Sackheim, R.K. Masse, Green propulsion advancement: Challenging the maturity of monopropellant hydrazine, J. Propul. Power 30 (2014) 265–276.

[2] C. H. Hwang, S. W. Baek, S. J. Cho, Experimental investigation of decomposition and evaporation characteristics of HAN-based monopropellants, Combust. Flame 161 (2014) 1109–1116.

[3] R. Amrousse, T. Katsumi, N. Itouyama, N. Azuma, H. Kagawa, K. Hatai, H. Ikeda, K. Hori, New HAN-based mixtures for reaction control system and low toxic spacecraft propulsion subsystem: Thermal decomposition and possible thruster applications, Combust. Flame 162 (2015) 2686–2692.

[4] R. Amrousse, T. Katsumi, N. Azuma, K. Hori, Hydroxylammonium nitrate (HAN)-based green propellant as alternative energy resource for potential hydrazine substitution: From lab scale to pilot scale-up, Combust. Flame 176 (2017) 334–348.

[5] A.A. Esparza, R.E. Ferguson, A. Choudhuri, N.D. Love, E. Shafirovich, Thermoanalytical studies on the thermal and catalytic decomposition of aqueous hydroxylammonium nitrate solution, Combust. Flame 193 (2018) 417–423.

[6] E.J. Wucherer, S. Christofferson, Assessment of high performance HAN-monopropellants, 36th AIAA/ASME/SAE/ASEE Joint Propulsion Conference, 16-19 July 2000, Huntsville, AL, paper AIAA-2000-3872.

[7] A.J. Brand, W. Drake, Energetic hydrazinium salts, Patent US 6,218,577, 2001.

[8] U. Swami, K. Senapathi, K. M. Srinivasulu, J. Desingu, A. Chowdhury, Ignition delays of mixtures of the non-hypergolic energetic ionic liquid hydroxyethylhydrazinium nitrate blended with unsymmetrical dimethylhydrazine, Propellants Explos. Pyrotech. 44 (2019) 1139–1146.

[9] U. Swami, K. Senapathi, K. M. Srinivasulu, J. Desingu, A. Chowdhury, Energetic ionic liquid hydroxyethylhydrazinium nitrate as an alternative monopropellant, Combust. Flame, 215 (2020) 93–102.

[10] A.J. Alfano, J.D. Mills, G.L. Vaghjiani, Resonant laser ignition study of HAN-HEHN propellant mixture, Combust. Sci. Technol. 181 (2009) 902–913.

[11] J.L. Shamshina, M. Smiglak, D.M. Drab, T.G. Parker, H.W.H. Dykes Jr., R. Di Salvo, A.J. Reich, R.D. Rogers, Catalytic ignition of ionic liquids for propellant applications, Chem. Commun. 46 (2010) 8965–8967.

[12] A. Chowdhury, S.T. Thynell, Kinetics of decomposition of energetic ionic liquids, Propellants Explos. Pyrotech. 35 (2010) 572–581.

[13] T. Ozawa, A new method of analyzing thermogravimetric data, Bull. Chem. Soc. Jpn. 38 (1965) 1881–1886.

[14] J.H. Flynn, L.A. Wall, A quick, direct method for the determination of activation energy from thermogravimetric data, J. Polym. Sci. B 4 (1966) 323–328.

[15] ASTM E1641-18, Test method for decomposition kinetics by thermogravimetry using the Ozawa/Flynn/Wall Method, ASTM Int., West Conshohocken, PA, 2018.

[16] ASTM E698-18, Test method for kinetic parameters for thermally unstable materials using differential scanning calorimetry and the Flynn/Wall/Ozawa method, ASTM Int., West Conshohocken, PA, 2018.

[17] H.E. Kissinger, Variation of peak temperature with heating rate in differential thermal analysis, J. Res. Natl. Bur. Stand. 57 (1956) 217–221.

[18] H.E. Kissinger, Reaction kinetics in differential thermal analysis, Anal. Chem. 29 (1957) 1702–1706.

[19] ASTM E2890-12, Standard test method for kinetic parameters for thermally unstable materials by differential scanning calorimetry using the Kissinger method, ASTM Int., West Conshohocken, PA, 2018.

[20] I.V. Arkhangel'skii, A.V. Dunaev, I.V. Makarenko, N.A. Tikhonov, S.S. Belyaev, A.V. Tarasov, Non-Isothermal Kinetic Methods, Max Planck Research Library for the History and development of Knowledge, Textbooks 1, Edition Open Access, Berlin, 2013.

[21] M.A. Bohn, Problems and faulty uses with the Prout–Tompkins description of autocatalytic reactions and the solutions, J. Therm. Anal. Calorim. 116 (2014) 1061–1072.

[22] P.J. Linstrom, W.G. Mallard (Eds.), NIST Chemistry WebBook, NIST Standard Reference Database Number 69, National Institute of Standards and Technology, Maryland, 2018

[23] J.C. Howard, G. Gever, A.B. Neill, P.H.L. Wei, The thermal decomposition of 2-hydrazinoethanol and 1-hydrazino-2-propanol, J. Org. Chem. 26 (1961) 1082–1083.

[24] Chemical Properties of 2-Hydroxyethylhydrazine (CAS 109-84-2), https://www.chemeo.com/cid/21-880-1/2-Hydroxyethylhydrazine.

2. Combustion of Aqueous HAN/Methanol Propellants at High Pressures

2.1. Introduction

Currently, chemical propulsion for space applications relies on highly toxic propellants such as hydrazine and its derivatives. The replacement of hydrazine by monopropellants based on hydroxylammonium nitrate (HAN, NH_3OHNO_3) is of great interest today because of their relatively low toxicity, high density, high specific impulse, and low freezing point [1-3]. HAN-based propellants are also of interest for other applications, including those involving higher pressures than in currently used thrusters.

HAN-based monopropellants include a fuel component that reacts with HAN decomposition products during combustion of the propellant, leading to a high specific impulse. Various fuels have been considered. For example, triethanolammonium nitrate (TEAN) was the fuel additive to HAN in liquid gun propellants [4-8]. For space propulsion, methanol, ethanol, propanol, butanol, glycine, and 2-hydroxyetylhydrazinium nitrate have been explored [9]. Currently, monopropellants based on HAN and methanol are being investigated extensively [2, 3].

However, the combustion mechanisms of HAN-based monopropellants are not well understood, especially at high pressures. Prior studies on the combustion of aqueous HAN solutions and their mixtures with TEAN, monoethanolamine nitrate (EAN), and glycine [4-7, 10, 11] have revealed an abnormal effect of pressure on the burning rate, i.e. a negative pressure exponent, at certain ranges of pressures. To explain this effect, different hypotheses were proposed, such as a change in the chemistry of HAN decomposition with pressure [4] and hydrodynamic instabilities [5].

More recently, several research teams focused on HAN/methanol/water propellants. Chang et al. [12] have studied their combustion in the pressure range 0.74−6.4 MPa. For the composition with 69.7% HAN, 14.79% methanol, 14.91% water, and 0.60% ammonium nitrate, they reported five pressure dependencies of the burning rate: a steady increase with increasing pressure from 0.8 to 1.13 MPa, a sharp increase at 1.13−1.27 MPa, a slight increase at 1.27−1.93 MPa, a plateau at 1.93−2.84 MPa, and a slow decrease at 2.84−6.4 MPa.

Katsumi et al. [13-15] have studied combustion of seven aqueous HAN solutions with HAN concentrations from 50 to 95% as well as two HAN/methanol/water propellants with different amounts of methanol and a small amount of ammonium nitrate at pressures 1–10 MPa. Depending on the concentration of HAN, different combustion modes were observed.

McCown and Petersen [16] have investigated combustion of HAN/water and HAN/methanol/water mixtures in a strand burner at pressures from 3 to 22 MPa. With increasing pressure from 3 to 5 MPa, the linear burning rate of 82.4% HAN solution increased by an order of magnitude. With further increase in pressure up to 22 MPa, it gradually decreased. The addition of 14.9% methanol dramatically increased the burning rate in the low part of the tested pressure range. The burning rate was independent of pressure in the range of 3−4.8 MPa. At higher pressures, five different pressure regimes were observed. At 4.8−10.8 MPa the burning rate

decreases with increasing pressure. Between 10.8 and 19.4 MPa, the burning rate first increases, then remains constant, and finally decreases. At 19.4−22 MPa it remains constant.

It is hard to explain the observed multiplicity of pressure regimes because the combustion mechanisms of HAN-based monopropellants involve interactions of various thermal and hydrodynamic processes with a complicated chemistry. Despite the voluminous literature on the kinetics of HAN decomposition (see, for example, references in [17]), the reaction mechanisms are not fully understood [18]. Although the global reaction is often given by:

$$4NH_3OHNO_3 \rightarrow 3N_2O + 2HNO_3 + 7H_2O, \quad (2\text{-}1)$$

HAN decomposition produces several other species, and a widely accepted mechanism of HAN decomposition includes the following steps:

$$NH_3OHNO_3 \rightarrow NH_2OH + HNO_3 \quad (2\text{-}2)$$

$$NH_2OH + HNO_3 \rightarrow HNO + HNO_2 + H_2O \quad (2\text{-}3)$$

$$NH_2OH + HNO_2 \rightarrow N_2O + 2\ H_2O \quad (2\text{-}4)$$

$$NH_2OH + HNO \rightarrow N_2 + 2\ H_2O \quad (2\text{-}5)$$

$$HNO + HNO_3 \rightarrow 2\ HNO_2 \quad (2\text{-}6)$$

$$HNO_2 + HNO_3 \rightarrow 2\ NO_2 + H_2O \quad (2\text{-}7)$$

$$2\ HNO \rightarrow N_2O + H_2O \quad (2\text{-}8)$$

$$3\ HNO_2 \rightarrow 2\ NO + HNO_3 + H_2O \quad (2\text{-}9)$$

Experimental studies of HAN decomposition have clearly demonstrated its autocatalytic behavior though the details of the autocatalytic mechanism are still under investigation [18]. In general, it is possible to conclude that a significant level of understanding has been achieved for the decomposition of HAN, but the effect of pressure on this process remains unclear.

The objective of the present work was to clarify the combustion mechanisms of HAN/methanol/water mixtures at high pressures, including the expansion of the tested pressure range to 30 MPa. The work included strand burner experiments with these mixtures and high-pressure differential scanning calorimetry of HAN decomposition.

2.2. Experimental

Decomposition of aqueous HAN solution (24 wt% HAN, 99.999% pure, Sigma-Aldrich) was studied using a high-pressure differential scanning calorimeter (Netzsch DSC 204 HP Phoenix). An alumina crucible with 10 μL of the HAN solution was heated at a rate of 10 ºC/min in a nitrogen environment. Prior to heating, three vacuum cycles were performed to evaporate water from the solution and to purge air from the furnace. The experiments were conducted at gauge pressures from 0 to 15 MPa (the maximum pressure in the instrument). Three to five tests were performed for each pressure. Constant pressure was maintained with two mass flow meters (SLA5800 Series,

Brooks Instruments). Correction runs for all crucibles and pressures were carried out prior to the DSC tests.

Using a strand burner (Design Integrated Technology, Inc.), combustion experiments were conducted with a mixture of 70.1 wt% HAN, 15.0 wt% water, and 14.9 wt% methanol, i.e. the same composition as in [16]. The same aqueous solution as in the DSC tests was used as a source of HAN. The mixture preparation included increasing the concentration of HAN in the solution to 82.4 wt%, which corresponds to the water/(HAN+water) mass ratio in the desired propellant composition. This was achieved by evaporation of water in a vacuum desiccator connected to a vacuum pump. The solution was then mixed with anhydrous methanol (Sigma-Aldrich).

The mixture was placed into a quartz tube (7 mm ID, 9 mm OD), one end of which was closed using epoxy. Two fuse wires (0.25 mm diameter, BFW-1/2 Cooper Bussmann) were inserted through holes in the tube wall, drilled 88.9 ± 1.6 mm apart. To ignite the mixture, a nichrome wire (0.51 mm diameter) was inserted through a third hole in the tube, approximately 1 cm above the first fuse wire. The holes were sealed with epoxy, and the tube with the sample was installed in a test cell, which was then filled with nitrogen at desired pressure. The strand burner is equipped with a temperature-maintaining liquid bath and a thermostat, which was set to 25 °C. Pressurizing the system with nitrogen raised the temperature to 70 °C or more, and the ignition was conducted after cooling to a temperature of 29–35°C in the reaction cell. As the combustion front propagates downward, the fuse wires break, starting and then stopping a timer. The average linear burning rate was determined based on the distance between the wires and the recorded time.

The melting point of the fuse wire was measured using a differential scanning calorimeter (Netzsch DSC 404 F1 Pegasus). An alumina crucible containing 11 mg of fuse wire was heated up to 800 ºC at a rate of 10 ºC/min in an argon flow.

2.3. Results

2.3.1. Differential scanning calorimetry of HAN decomposition at high pressures

Figure 2-1 shows the plot of the DSC peak temperature as a function of absolute pressure. The peak temperature at atmospheric pressure was close to the value reported in [17]. It is seen that the peak temperature decreases by about 50 °C with increasing pressure from 0.1 to 2.1 MPa and remains about the same (around 130 °C) with further increase in pressure.

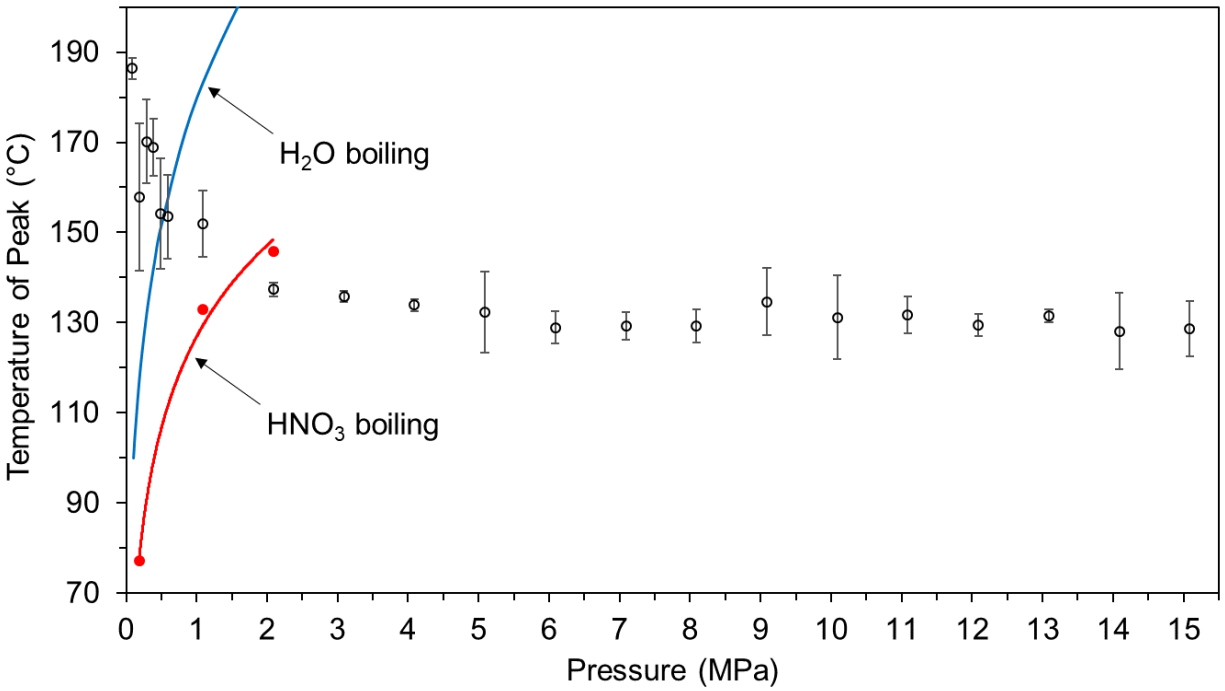

Fig. 2-1. Temperature of the DSC peak vs. absolute pressure; heating rate: 10 ºC/min. Lines show saturated temperatures of nitric acid and water.

Pressure also affected the shape of the DSC curves. Figure 2-2 shows the curves obtained at absolute pressures of (a) 0.2 MPa and (b) 8.1 MPa. It is seen that at 0.2 MPa the peaks are relatively broad and there is a large scatter in the peak temperatures (this results in the largest error bar in Fig. 2-1). In contrast, at 8.1 MPa the peaks are sharp, i.e. the exothermic effect is concentrated in a much smaller temperature range, and the scatter is smaller (the color in these plots is used to see the curves clearer).

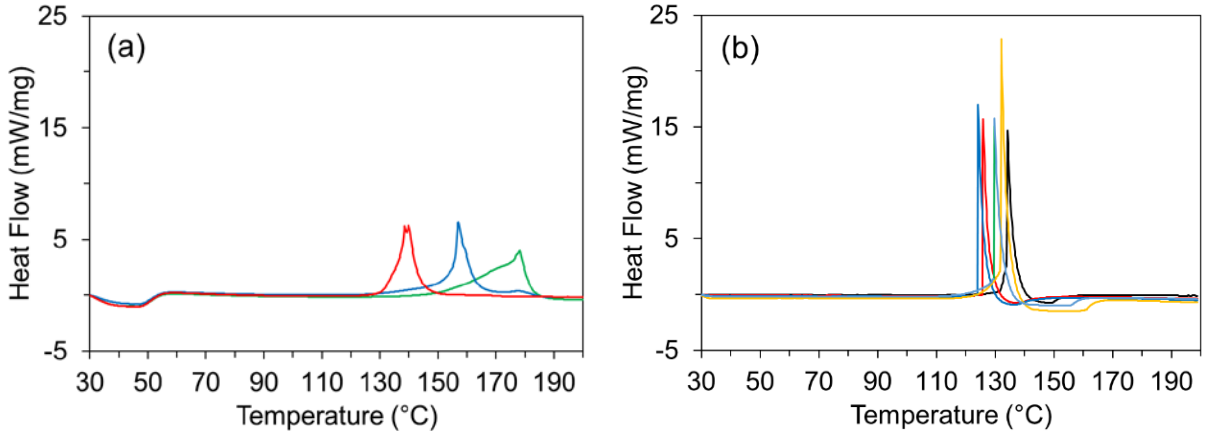

Fig. 2-2. DSC curves for decomposition of HAN at absolute pressures (a) 0.2 MPa and (b) 8.1 MPa.

2.3.2. Combustion of HAN/methanol/water propellants at high pressures

The strand burner tests were performed over the range of gauge pressures from 8 to 30 MPa at 1 MPa intervals, with three tests conducted at each pressure. Tests were also performed at 12.5 and 13.5 MPa to obtain more information on the combustion behavior in this pressure range. In the tests conducted at gauge pressures 9–30 MPa, successful ignition led to breaking the fuse wires. A few drops of yellowish liquid often remained in the sample tube after a test. Two tests were conducted at a gauge pressure of 8 MPa. In both tests, the fuse wires were not broken though most of the liquid disappeared (approximately 1 cm, i.e. 0.4 mL, of the yellow liquid was found on the bottom of the tube). No testing was conducted at pressures below 8 MPa.

Figure 2-3 shows the linear burning rate as a function of absolute pressure. Error bars indicate a standard deviation from the mean of the three tests that were conducted at a given pressure. It is seen that with increasing pressure from 9 to 12 MPa, the burning rate decreases according to the following power law:

$$r_b = 776.02P^{-0.75} \tag{2-10}$$

where r_b is the burning rate in mm/s and P is the absolute pressure in MPa. With increasing pressure from 12 to 14 MPa, the burning rate significantly increased. At 14–19 MPa no pressure effect was observed and the average burning rate was 189 mm/s. At 20 MPa the burning rate decreased to 165±3 mm/s, i.e. by 13% (see Fig. 2-3). Finally, the dependence at 22–30 MPa shows a clear increase described by the following power law:

$$r_b = 2.3361P^{1.3511} \tag{2-11}$$

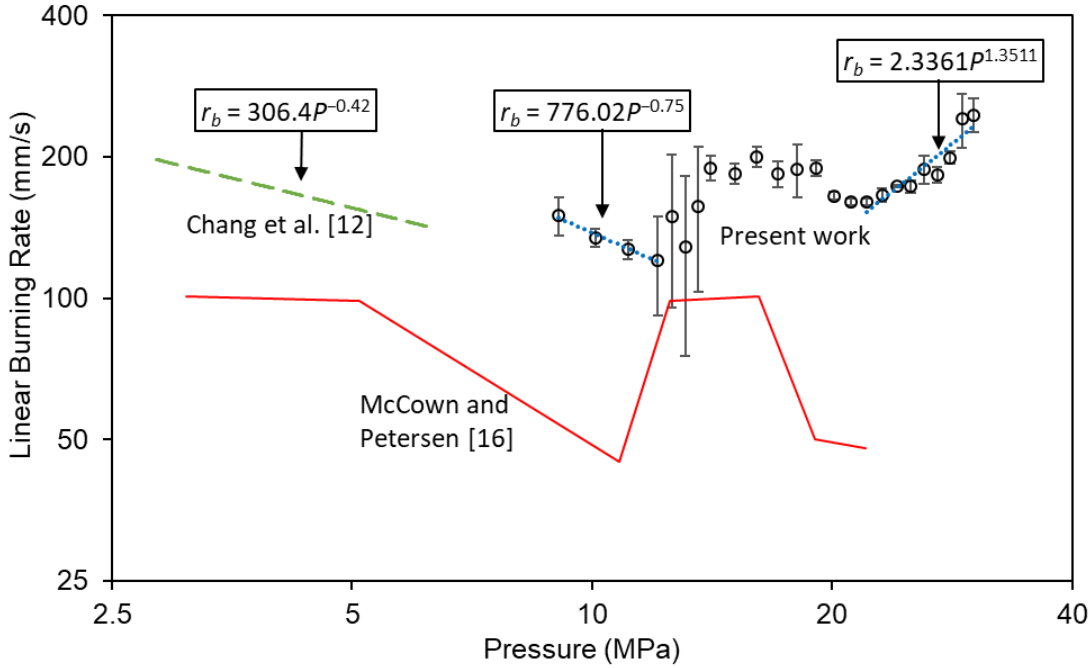

Fig. 2-3. Linear burning rate of HAN/methanol/water propellant vs. pressure in the present work (points), in [16] (solid line), and in [12] (dashed line).

It is worth noting that at 12.1–13.6 MPa, very different burning rates were observed at each tested pressure, leading to huge standard deviations in Fig. 3. To clarify why this scatter took place, Figure 2-4 shows the actual measured values at 9–19 MPa (two points overlap at 13.1 MPa). It is seen that the burning rate at each pressure in the range of 12.1–13.6 MPa was either low or high. This indicates that 12.1–13.6 MPa is a transition region from the slower combustion regime (A) to the faster one (B). Apparently, in each test, small variations of the experimental conditions could affect the process, resulting in either regime A or regime B.

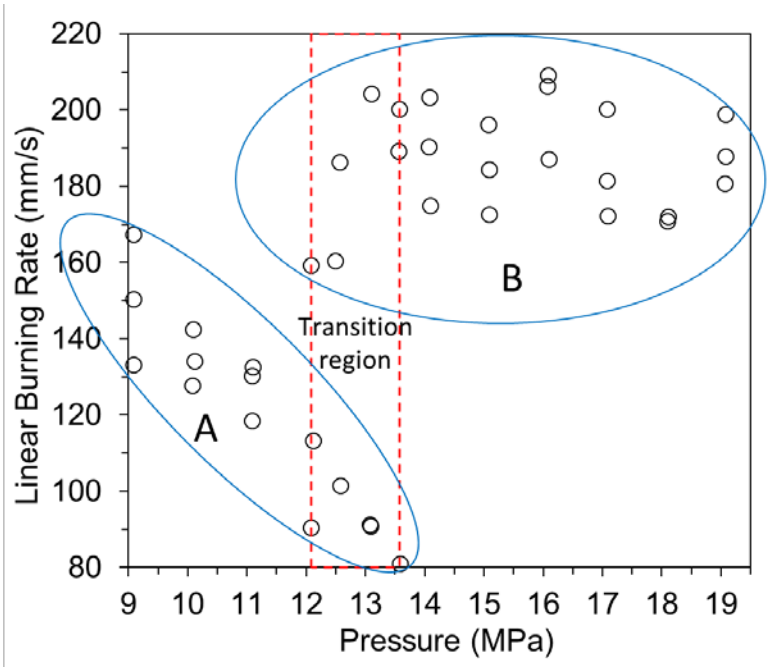

Fig. 2-4. Linear burning rate of HAN/methanol/water propellant vs. pressure in the range 9–19 MPa (actual data points).

2.4. Discussion

The 50 °C decrease in the decomposition temperature of HAN with increasing pressure from atmospheric to 2 MPa and no substantial change at higher pressures are important observations (Fig. 1). It is also notable that the DSC peak was broad at low pressures and sharp at high ones. The absence of any significant pressure effect beyond 2 MPa indicates that the chemical mechanism of the decomposition is insensitive to pressure. The accelerating effect of pressure can be explained by the effect of pressure on the evaporation of products that form and react during the decomposition process. The first step of HAN decomposition, described by Eq. (1), produces nitric acid (HNO_3), which plays a critical role in the reaction mechanism [18]. The loss of nitric acid by evaporation inhibits the reactions. An increased pressure suppresses the evaporation, promoting the reactions and leading to a decreased temperature of decomposition and sharper DSC peaks. To verify this explanation, the boiling point of nitric acid (65 wt% aqueous solution) was determined with DSC tests at gauge pressures of 0, 1, and 2 MPa. The obtained dependence is

shown in Fig. 1. It is seen that the HNO_3 boiling curve separates the areas with higher and lower decomposition temperatures, which supports the proposed explanation of the pressure effect.

In addition, although water is not involved as a reactant in the reaction mechanism described by Eqs. (2−9), it has been previously reported that water decreases the induction period of solid HAN [19]. Figure 1 shows that at pressures below 0.5 MPa the peak temperature is higher than the boiling point of water, while at higher pressures it is the opposite. Therefore, the formation of liquid water during the reaction at high pressures may also play a role in decreasing the decomposition temperature.

The strand burner experiments with HAN/water/methanol mixtures have revealed information that helps understand prior results and clarify the combustion mechanisms. For comparison, Figure 3 shows the dependences obtained in [12, 16]. It is seen that there are some similarities with the prior results. The dependence obtained in the present work exhibits a negative pressure exponent at relatively low pressures, similar to both [12] and [16]. With further increase in pressure, a drastic rise of the burning rate followed by a plateau was observed in both the present work and [16]. However, the burning rates in [16] were much lower than in the present work and [12]. This is explained by the incorrect determination of the linear burning rate based on pressure rise data in [16], which included secondary gas phase reactions after the liquid regression was complete. Indeed, the same experimental setup was used for measuring the burning rates of aqueous HAN solutions [20, 21], but the authors also conducted video recording, which revealed that pressure continued to increase after the liquid had been burned out. This indicates that the reactions in the gas phase still occur after the liquid-gas interface has reached the bottom of the tube. The formation of a reactive gas mixture during combustion of a HAN/methanol-based propellant was also seen in [12], where video recording has shown that after the liquid sample had burned out, the dark products in the tube were ignited by the heated nichrome wire, resulting in a downward propagating flame.

The sharp increase in the burning rate by over 50 % at around 13 MPa is a remarkable result. This cannot be caused by a decreased temperature of HAN decomposition because the DSC studies of the aqueous HAN solution have not shown any effect of pressure on the decomposition at 5–15 MPa. The dramatic increase in the burning rate can be explained by reaching the critical pressure of the liquid mixture.

Indeed, video recording of the decomposition process in aqueous HAN solutions [5] has revealed phenomena that can be explained by approaching the critical point of the liquid mixture. It was reported that at low pressure (6 MPa) the liquid-gas interface forms a meniscus, which becomes less pronounced with increasing pressure and completely disappears at 13 MPa. The changes of the meniscus were explained by hydrodynamic instabilities due to the different densities of liquid and the decomposition products. However, they could also be caused by the changes of the surface tension with approaching the critical point.

The pseudocritical pressure (P_{cm}) and temperature (T_{cm}) of the used methanol/water/HAN mixture were calculated using the corresponding-states method and specifically the Prausnitz-Gunn expressions [22]:

$$T_{c,m} = \sum_j y_j T_{cj} \quad (2\text{-}12)$$

$$P_{cm} = T_{cm}\left(\sum_j \frac{y_j P_{cj} V_{cj}}{T_{cj}}\right)\left(\sum_j y_j V_{cj}\right)^{-1} \quad (2\text{-}13)$$

where y_j, T_{cj}, P_{cj}, and V_{cj} are, respectively, the mole fraction, the critical temperature, the critical pressure, and the critical molar volume of the component "*j*". Table 2-1 shows the critical pressures, temperatures, and molar volumes of the mixture components, used in the calculations. The mole fractions of methanol, water, and HAN in the studied mixture are 0.229, 0.411, and 0.360. The obtained values of P_{cm} and T_{cm} are 10.5 MPa and 658 K, respectively.

Table 2-1. Critical point properties of the mixture components.

Component	P_c	T_c	V_c	**Ref.**
	MPa	K	$cm^3 \cdot mol^{-1}$	
Methanol	8.1	513	117	[23]
Water	22.1	647	56	[23]
HAN	7.7	763	196	[24]

The obtained value of the critical pressure, 10.5 MPa, is lower than the pressure range 12.1–13.6 MPa where the burning rate increased. However, the critical parameters of HAN, used in the calculations, were calculated in work [24] with no experimental verification, and it is possible that the actual parameters are different. In addition, the corresponding states method may led to errors [22]. Although for binary methanol/water mixtures it produces the values that are relatively close to the actual critical parameters [25], the accuracy of this method in applications to mixtures with ionic liquids, such as HAN, has not been evaluated yet.

If the mixture becomes a supercritical fluid at 12.1–13. 6 MPa, the observed increase in the burning rate can be explained as follows. At pressures below the critical pressure, the following processes occur in the combustion wave. HAN decomposes at a relatively low temperature as shown in the DSC tests. The produced gases (intermediate and final products of decomposition) form bubbles, which move up to the sample surface. Note that brown bubbles were observed during combustion of aqueous HAN solutions [14, 15]. The thermocouple measurements in [12] have shown that after the front has passed the thermocouple junction, the temperature remains constant (between the boiling points of methanol and water) for a long time with no subsequent rise. This was explained by the formation of a two-phase (liquid-gas) mixture that apparently occupied a relatively thick zone. In the present work, the fact that the wires were not broken at 8 MPa, provides information on possible temperatures. According to the manufacturer's datasheet, the wires were made of a lead/antimony alloy (98.25–98.75% Pb and 1.25–1.75% Sb) with solidus

and liquidus at 304 and 316 °C, respectively. The conducted DSC test has shown melting at 318 °C, i.e. close to the liquidus of the alloy. Therefore, at 8 MPa the maximum temperature in the combustion wave was lower than this value and possibly close to the boiling point of water (296 °C at 8.1 MPa). This indicates that the reactions between the oxidizing products of HAN decomposition and methanol do not form a gas-phase flame front and apparently occur in the two-phase zone on top of the regressing surface. This is in agreement with Vosen's results on the combustion of HAN/water/TEAN mixtures, where visible flame, detached from the surface, was observed only at pressures as high as 26.7–30 MPa [4].

The measurements of the burning rate for HAN/water/methanol mixtures have resulted in a pressure exponent of −0.744 at 9–12 MPa in the present work and −0.42 at 2.84–6.4 MPa in work [12]. As proposed by Vosen based on the video records of HAN/water and HAN/water/TEAN mixtures [4-6], the decrease in the burning rate with pressure can be associated with a decrease in the surface area of the liquid-gas interface (the meniscus).

At pressures above the critical pressure, the process is different. In the thermal profile of the combustion wave, when the critical temperature is reached, the mixture becomes a supercritical fluid, where no two-phase mixture is possible. Therefore, the temperature above this location is not limited by any boiling point. At a higher temperature, the reactions occur more rapidly, leading to a higher velocity of the combustion wave. Since the burning rate of aqueous HAN solution remained constant with increasing pressure beyond the point of meniscus' disappearance [5], it can be concluded that the acceleration in supercritical HAN/water/methanol mixtures is driven by the reactions between methanol and the decomposition products.

It should be noted that in the present work the sharp increase in the burning rate occurred at a slightly higher pressure than in [16]. This is likely a result of a much larger system volume in the present study (approximately 40 L, including the surge tank). Because of this volume difference, the typical results in [16] showed an increase in pressure of approximately 1.25 MPa during testing, compared with an average of 0.18 MPa in the present work. While the results [16] used the average pressure for a given test, it is possible that in the tests started at a pressure slightly lower than the critical one, the critical parameters were reached during the combustion, thus sharply increasing the burning rate and causing the apparent leftward shift in the burning rate – pressure dependence.

The plateau in this dependence at 14–19 MPa is understandable. Since the decrease in the burning rate, observed at lower pressure, was related to the changes in the meniscus, its disappearance eliminates the effect. Although the plateau was observed in both present work and [16], the results at higher pressures are different. The dependence [16] showed a decrease in the burning rate by approximately 50% at 16–19 MPa (see Fig. 3). In the present work, a decrease was observed at 20 MPa, but its magnitude was much smaller, about 13%. It is possible that this discrepancy may be associated with calculating the burning rate based on the time of the pressure rise in [16].

The maximum tested pressure in [16] was 22 MPa, while the present study was conducted up to 30 MPa, and this produced new results: a steady rise in the burn rate over the pressure range 22–30 MPa. It is interesting that for HAN/water/TEAN mixtures, the increase in the burning rate

with pressure was observed at pressures over 100 MPa [7]. The mechanism of this increase at high pressures remains unclear and worthy of further studies.

The obtained results may have important implications for propulsion. As noted in [12], sharp increases in the burning rate may explain rough combustion and pressure spikes observed in engine firing tests. Therefore, to prevent combustion instabilities in the propulsion systems using HAN-based propellants, pressure in the chamber should not be close to the critical pressure of the propellant.

2.5. Conclusions

High-pressure differential scanning calorimetry has shown that the decomposition temperature of HAN decreases by approximately 50 °C with increasing pressure from atmospheric to 2 MPa and remains virtually constant, around 130 °C, with further increasing pressure to 15 MPa. The lower decomposition temperature at high pressure is explained by suppressing evaporation of HNO_3 and H_2O that are formed during the decomposition process.

Strand burner experiments with an aqueous HAN/methanol solution (70.1 wt% HAN, 15.0 wt% water, and 14.9 wt% methanol) have revealed different pressure dependencies of the linear burning rate. A sharp increase by over 50% at 12−14 MPa was the most remarkable result. This effect was explained by reaching the critical pressure of the liquid, which changed the combustion process. Specifically, at a supercritical pressure, instead of a two-phase (liquid-gas) medium, a supercritical fluid exists in the combustion wave and the maximum temperature is not limited by boiling, leading to the acceleration of the reactions between methanol and the decomposition products.

Other observed pressure dependencies of the burning rate include a steady decrease at 9–12 MPa, a plateau at 14–19 MPa, a decrease by 13% at 20 MPa, and a steady increase at 22–30 MPa. The regime with a negative pressure exponent and the plateau can be explained by decreasing the surface area of the liquid-gas interface with approaching the critical point and by the absence of this interface at pressures above the critical point. Future studies should involve clarification of the combustion mechanisms at 19−30 MPa.

2.6. References

[1] R.L. Sackheim, R.K. Masse, Green propulsion advancement: Challenging the maturity of monopropellant hydrazine, J. Propuls. Power 30 (2) (2014) 265-276.

[2] R. Amrousse, T. Katsumi, N. Itouyama, N. Azuma, H. Kagawa, K. Hatai, H. Ikeda, K. Hori, New HAN-based mixtures for reaction control system and low toxic spacecraft propulsion subsystem: Thermal decomposition and possible thruster applications, Combust. Flame 162 (6) (2015) 2686-2692.

[3] R. Amrousse, T. Katsumi, N. Azuma, K. Hori, Hydroxylammonium nitrate (HAN)-based green propellant as alternative energy resource for potential hydrazine substitution: From lab scale to pilot scale-up, Combust. Flame 176 (2) (2017) 334-348.

[4] S.R. Vosen, The burning rate of hydroxylammonium nitrate-based liquid monopropellants, Proc. Combust. Inst. 22 (1) (1988) 1817-1825.

[5] S.R. Vosen, Concentration and pressure effects on the decomposition rate of aqueous hydroxylammonium nitrate solutions, Combust. Sci. Technol. 68 (4-6) (1989) 85-99.

[6] S.R. Vosen, Hydroxylammonium nitrate-based liquid propellant combustion—Interpretation of strand burner data and the laminar burning velocity, Combust. Flame 82 (3-4) (1990) 376-388.

[7] Y.-P. Chang, E. Boyer, K.K. Kuo, Combustion behavior and flame structure of XM46 liquid propellant, J. Propuls. Power 17 (4) (2001) 800-808.

[8] Y.J. Lee, T.A. Litzinger, Combustion chemistry of HAN, TEAN, and XM46, Combust. Sci. Technol. 141 (1-6) (1999) 19-36.

[9] E.J. Wucherer, S. Christofferson, B. Reed, Assessment of high performance HAN-monopropellants, in: 36th AIAA/ASME/SAE/ASEE Joint Propulsion Conference, Huntsville, AL, 2000, AIAA 2000-3872.

[10] B.N. Kondrikov, V.E. Annikov, V.Yu. Egorshev, T.T. De Luca, Burning of hydroxylammonium nitrate, Combust. Explos. Shock Waves 36 (1) (2000) 135-145.

[11] Y.-P. Chang, K.K. Kuo, Assessment of combustion characteristics and mechanism of hydroxylammonium nitrate-based liquid monopropellant, J. Propuls. Power 18 (5) (2002) 1076-1085.

[12] Y.-P. Chang, J.K. Josten, B.Q. Zhang, K.K. Kuo, Combustion characteristics of energetic HAN/methanol-based monopropellants, in: 38th AIAA/ASME/SAE/ASEE Joint Propulsion Conference, Indianapolis, IN, 2002, AIAA Paper 2002-4032.

[13] T. Katsumi, R. Matsuda, T. Inoue, N. Tsuboi, H. Ogawa, S. Sawai, K. Hori, Combustion characteristics of HAN-based liquid monopropellant," Int. J. Energ. Mater. Chem. Propuls. 7 (2008) 123-127.

[14] T. Katsumi, R. Matsuda, T. Inoue, N. Tsuboi, H. Ogawa, S. Sawai, K. Hori, Combustion characteristics of hydroxylammonium nitrate aqueous solutions, Int. J. Energ. Mater. Chem. Propuls. 9 (3) (2010) 219-231.

[15] T. Katsumi, T. Inoue, J. Nakatsuka, K. Hasegawa, K. Kobayashi, Sh. Sawai, K. Hori, HAN-based green propellant, application, and its combustion mechanism, Combust. Explos. Shock Waves 48 (5) (2012) 536-543.

[16] K.W. McCown, E.L. Petersen, Effects of methanol and fumed silica on linear burning rates of aqueous hydroxylammonium nitrate, Int. J. Energ. Mater. Chem. Propuls. 14 (1) (2015) 1-12.

[17] A.A. Esparza, R.E. Ferguson, A. Choudhuri, N.D. Love, E. Shafirovich, Thermoanalytical studies on the thermal and catalytic decomposition of aqueous hydroxylammonium nitrate solution, Combust. Flame, 193 (7) (2018) 417-423.

[18] K. Zhang, S.T. Thynell, Thermal decomposition mechanism of aqueous hydroxylammonium nitrate (HAN): Molecular simulation and kinetic modeling, J. Phys. Chem. A 122 (2018) 8086-8100.

[19] H. Lee, T.A. Litzinger, Thermal decomposition of HAN-based liquid propellants, Combust. Flame 127 (4) (2001) 2205-2222.

[20] J. Stahl, G. Homan-Cruz, E. Petersen, Comparison of liquid monopropellant burning rates from pressure data and high-speed video," in: 9th U.S. National Combustion Meeting, Cincinnati, OH, 2015.

[21] J.C. Thomas, G.D. Homan-Cruz, J.M. Stahl, E.L. Petersen, The effects of SiO_2 and TiO_2 on the two-phase burning behavior of aqueous HAN propellant, Proc. Comb. Inst. 37 (3) (2019) 3159–3166.

[22] B.E. Poling, J.M. Prausnitz, J.P. O'Connell, The Properties of Gases and Liquids, 5th ed., McGraw Hill, New York, 2001.

[23] NIST Chemistry WebBook, NIST Standard Reference Database Number 69, National Institute of Standards and Technology, available at https://webbook.nist.gov.

[24] M.E. Kounalakis, G.M. Faeth, Combustion of HAN-based monopropellants near the thermodynamic critical point, Combust. Flame 74 (2) (1988) 179-192.

[25] C. Xiao, H. Bianchi, R. Tremaine, Excess molar volumes and densities of (methanol + water) at temperatures between 323 K and 573 K and pressures of 7.0 MPa and 13.5 MPa, J. Chem. Thermodyn. 29 (3) (1997) 261-286.

3. Combustion of Gelled HAN/Methanol/Water Propellants

3.1. Introduction

Green monopropellants based on energetic ionic liquids, such as hydroxylammonium nitrate (HAN, $NH3OH^{+}NO3^{-}$), are being investigated as a potential replacement for highly toxic hydrazine in space propulsion applications. HAN-based monopropellants combine the advantages of reduced toxicity, low freezing point, high density, and high specific impulse [1]. While HAN itself decomposes exothermically, it is typically used as an oxidizer mixed with a fuel component to increase the specific impulse. Such fuel components include triethanolammonium nitrate (TEAN) [2-4], glycine [5], 2-hydroxyethylhydrazinium nitrate (HEHN) [6], and methanol [7-10]. The present work focuses on the HAN/methanol pair as it is used in SHP163, one of the most promising green monopropellants [11], and there exists a large volume of data on this propellant in the open literature.

Combustion of HAN/methanol propellants has demonstrated significant fluctuations of the burning rate at elevated pressures. Chang et al. reported two distinct burning regimes in the pressure range 0.8 – 7 MPa for a mixture of 77.25 wt% HAN, 0.67 wt% ammonium nitrate (AN), 17.19 wt% methanol, and 4.89 wt% water, with a transition at approximately 2.9 MPa [7]. For a mixture of 69.70 wt% HAN, 0.60 wt% AN, 14.79 wt% methanol, and 14.91 wt% water, five regimes were identified, including two with a negative pressure exponent. Note that the latter mixture contained 3 times more water, while the other components maintained the same mass ratios.

Katsumi et al. conducted testing of SHP163 (73.6 wt% HAN, 3.9 wt% AN, 6.2 wt% water, and 16.3 wt% methanol) at pressures up to 7 MPa [8]. In contrast to a control composition without methanol, the SHP163 samples exhibited low burning rates at the tested pressures. In addition, the burning rates increased steadily with increasing pressure, while the control composition showed a sudden increase at around 3 MPa. This sudden increase was explained based on the images of the reacting mixture. At slower burning rates, a liquid/gas transition region was seen with small bubbles from HAN decomposition. At faster burning rates, however, larger bubbles evolved which pushed into the liquid region. The authors theorized that because the HAN decomposition reactions could proceed farther inside these larger bubbles, the liquid region became superheated, leading to ever more bubble production and hydrodynamic instabilities. This increased the size of the liquid-gas interface, and, in turn, caused the increase in the apparent linear burning rate.

McCown and Petersen studied combustion of an aqueous HAN solution (82.4 wt% HAN) and an aqueous HAN/methanol mixture (70.1 wt% HAN, 14.9 wt% methanol) at pressures up to 22 MPa [9]. The aqueous HAN solution exhibited a significant increase in burning rate at pressures up to 5 MPa, followed by a decreasing burning rate with increasing pressure beyond this value. The addition of methanol, however, greatly increased the burning rate at pressures below 5 MPa and resulted in six burning regimes over the total range of pressures. Four of these regimes had negative pressure exponents.

Ferguson et al. studied an identical aqueous HAN/methanol mixture at pressures 8 – 30 MPa [10]. Roughly five distinct pressure regimes were identified, in a similar pattern to that in work [9]. The pressure range of 12 – 14 MPa was characterized as a transition region where the mixture becomes a supercritical fluid, leading to a rapid increase in the burning rate. High-pressure differential scanning calorimetry (HPDSC) revealed a decrease in the temperature of peak decomposition as pressure increased to 2 MPa, followed by stabilization at 2 – 15 MPa. This was explained by the increased boiling point of nitric acid (HNO_3), which is commonly considered a key intermediate product of HAN decomposition.

While the decomposition of HAN and characteristics of HAN-based liquid propellants have been studied extensively, little is known about the potential effect of gelling on their combustion. The addition of a gellant to a liquid propellant increases the viscosity, creating a shear thinning, thixotropic fluid [12]. A gelled propellant combines many advantages of solid and liquid propellants [12, 13]. For instance, the high viscosity enables the addition of energetic or catalytic particles to the liquid propellant by preventing particle sedimentation. Owing to these advantages, gelled propellants are being studied currently, and the investigated systems include ionic liquids [14]. However, the information on gelled HAN-based propellants is scarce. McBratney gellified XM46 (a HAN/TEAN-based propellant) and 9.1 M aqueous HAN using 1 wt% Rhamsam, and tested them in a strand burner at pressures up to 300 MPa [15]. It was shown that the gelled aqueous HAN solution exhibited a consistent increase in the burning rate with increasing pressure from 30 to 180 MPa, but the gelled HAN/TEAN propellant exhibited two burning regimes, with a transition at roughly 70 MPa.

Sabourin et al. showed that nitromethane gelled with CAB-O-SIL (primarily SiO_2) increased the burning rate to a maximum at 1 – 3 wt% loading, before falling again with increasing concentration [16]. The authors also reported that the use of the SiO_2 gellant reduced the pressure exponent when compared to pure nitromethane.

Kondrikov et al. studied a mixture of HAN and monoethanolamine nitrate (EAN) and a 64 wt% aqueous HAN solution, both ungelled and gelled with polyacrylamide [17]. The ungelled version exhibited rapid burning rates (greater than 200 mm/s) with a weak pressure dependence. The gelled version burned slower in comparison, with a rapid increase in burning rate at pressures up to approximately 8 MPa, then increasing slightly with additional pressure.

Thomas et al. gelled an 82.4 wt% aqueous HAN solution with fumed silica or titania particles in concentrations of 1 or 3 wt% [18]. Fumed silica at 1 wt% increased the regression rate at lower pressures (below 10 MPa) and the overall burning rate (including gas-phase reactions in the chamber after decomposition of the entire liquid sample) at all pressures. The titania particles at 1 wt% only affected the overall burning rate at pressure below 5.7 MPa (i.e., the liquid regression rate appeared unaffected). Notably, increasing the silica content from 1 to 3 wt% resulted in a further increase in the burning rate; this effect was not observed with titania particles. While not explicitly stated, both additives appeared to decrease the pressure exponent in the affected pressure ranges, similar to the results seen with nitromethane [16]. The authors eliminated chemical,

rheological, and thermal effects of the additives on the burning rate and proposed a catalytic response as the cause for the increase in burning rates.

It is clear from this brief review that HAN-based monopropellants exhibit significant variations in burning rates with pressure. Generally, the addition of a gelling agent appears to reduce or eliminate these fluctuations, but the cause remains unknown. The objective of the present study was to examine the effect of gelling on the combustion behavior of an aqueous HAN/methanol propellant. As in the work [17], polyacrylamide (PAM) was used as the gellant. This organic polymer has been widely used to make water gels and, more recently, to prepare stable, combustible metal/water mixtures [19-23]. An important advantage of PAM is its decomposition at temperatures lower than those in rocket engines [22]. Although many oxidizers react with organic gellants [13], the reactivity of HAN in an aqueous solution (i.e., before decomposition) is low, and the mixture remains stable after gelling with PAM.

In the present work, the gelled HAN/methanol/water mixtures were ignited in a nitrogen environment at pressures up to 30 MPa. Thermoanalytical studies were also conducted to investigate effects of the gellant on the decomposition of HAN in the mixture, both at atmospheric and elevated pressures.

3.2. Experimental

HAN (24 wt% aqueous solution), polyacrylamide, and anhydrous methanol were purchased from MilliporeSigma. The PAM and methanol were used as received. Water was removed from the aqueous HAN solution in a desiccator connected to a vacuum pump until the concentration of HAN reached 82.4 wt%. A mixture of 70.1 wt% HAN, 15.0 wt% water, and 14.9 wt% methanol was produced by adding methanol to the 82.4 wt% aqueous HAN solution. An additional 1 wt% PAM was added to the liquid and mixed in a resonant acoustic mixer (Resodyn LabRAM) to create a viscous gel.

Combustion testing was conducted in a strand burner (Design Integrated Technology, Inc.), which has a maximum operating pressure of 5000 psi (34.5 MPa). A thermal bath was used to maintain the initial temperature at approximately 25 °C. The sample was ignited by a nichrome wire (0.5 mm diameter). In each test, an average linear burning rate was determined using two breaking fuse wires (0.25 mm diameter, BFW-1/2 Cooper Bussman, 89 mm apart) that started and stopped a timer on the strand burner control console. To test liquid or gelled mixtures, a quartz tube (7 mm ID, 9 mm OD) was used. Holes were drilled in the tube for the nichrome and fuse wires, and the holes and bottom were sealed with epoxy (J-B Weld ClearWeld). A minimum of three combustion tests were conducted at even number intervals over the pressure range 4 – 24 MPa. At least one test was conducted at intervals of 1 MPa over the range 4 – 30 MPa.

Thermoanalytical experiments were conducted in a thermogravimetric analyzer (Netzsch TG 209 F1 Iris), a differential scanning calorimeter (Netzsch DSC 404 F1 Pegasus), and a high-pressure differential scanning calorimeter (Netzsch DSC 204 HP Phoenix). All experiments were performed using alumina crucibles (85 μL) without lids. For TGA and DSC at atmospheric

pressure, a helium environment was used to facilitate evolved gas analysis, while nitrogen was used for the HPDSC experiments. Prior to a linear heating program, a 10 min isothermal step with 100 mL/min purge gas was used to replace residual air. In the TGA and DSC at atmospheric pressure, the gas flow rate during the heating program was set to 25 and 20 mL/min, respectively. HPDSC experiments were conducted at absolute pressures 0.6, 1.1, 2.1, 5.1, 10.1, and 15.1 MPa. They were conducted under static conditions, although some gas flow occurred throughout the tests because of the pressure stabilization. The TGA, DSC, and HPDSC experiments were conducted at a heating rate of 10 °C/min.

Prior to testing, all the instruments were calibrated using melting point standards. A correction run with an empty crucible was performed before the sample was tested to determine the baseline curve for the specific conditions of the test. Three tests were conducted in the TGA and DSC at atmospheric pressure; three tests were also conducted at each of the listed pressures in the HPDSC. In several DSC tests, a mass spectrometer (Netzsch QMS 403D Aëolos, electron ionization) was connected to the DSC via a heated (150 °C) capillary line. This allowed for near real time detection of the product gases during the heating program.

3.3. Results and Discussion

3.3.1 Combustion experiments

Figure 3-1 shows the obtained dependence of the linear burning rate of gelled aqueous HAN/methanol propellant on absolute pressure. For comparison, the figure also shows the results for an ungelled version of this propellant [10], obtained in the same strand burner. Error bars represent one standard deviation from the average at each pressure. It is clear that gelling has suppressed the variety of burning regimes seen with increasing pressure in the ungelled propellant, and the propellant maintains a constant pressure exponent throughout the tested pressure range. The obtained pressure dependence of the burning rate is:

$$r_b(mm/s) = (4.55 \pm 1.13)[P(MPa)]^{(1.15 \pm 0.05)} \quad (3\text{-}1)$$

where the error bands were determined by applying a LINEST function of Excel.

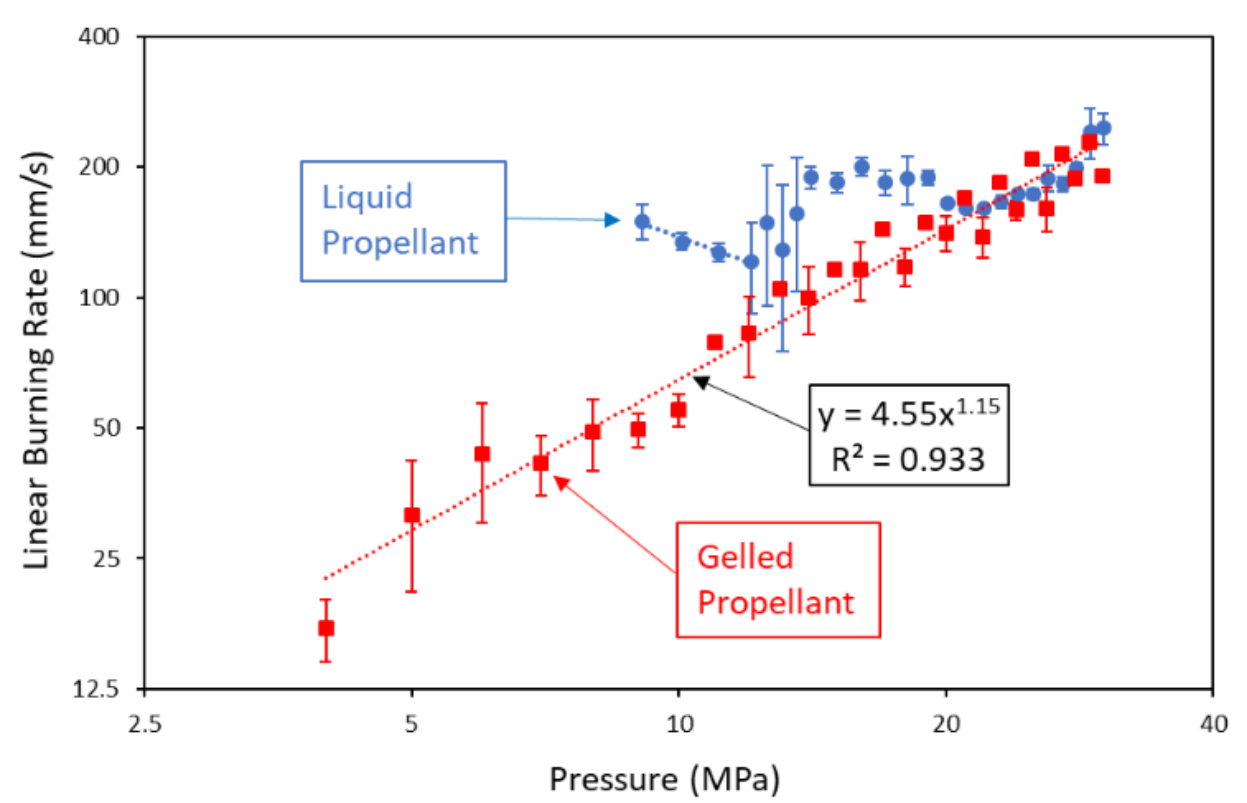

Fig. 3-1. Linear burning rates of gelled aqueous HAN/methanol propellant (red squares) and ungelled propellant (blue circles) [10].

It should be noted that burning rates for the gelled mixture were determined at pressures as low as 4 MPa. In the test at 3 MPa, no data was produced as the fuse wires did not break. Apparently, the temperature of the combustion front was not high enough to break the fuse wires, which melted at 318 °C according to the conducted DSC [10].

Figure 3-2 shows sample tubes after combustion at pressures 4 – 9 MPa. At 4 MPa, the sample tube interior was coated with a thick black residue. With increasing pressure, this residue became thinner, until disappearing at pressures beyond 10 MPa. This residue was not seen after testing the ungelled version of the propellant. As the fuse wires were broken in these tests, the temperature of the combustion front exceeded 318 °C in all of them.

Fig. 3-2. Sample tubes after combustion of the gelled propellant mixture at pressures: from left to right, 4, 5, 6, 7, 8, and 9 MPa.

Let us consider the thermal decomposition of the PAM gellant. Polyacrylamide decomposes in a two-stage process. These stages have been reported as 330 and 400 °C, based on TGA analysis [24], which was separately confirmed [25]. A third study using MS determined peak gas evolution occurred first at 272 – 297 °C, and again at 374 – 384 °C [26]. A further peak of gas detection was observed at 481 – 572 °C. It should be noted that the polyacylamide decomposed completely by 700 °C; while not explicitly stated, the TGA curve implied complete mass loss of PAM. In examining the residue in the present study, at 4 MPa the temperature may be well below 400 °C, which is needed for the second stage of PAM decomposition, so the black residue forms. As the pressure, and therefore the temperature in the combustion front, increase, the residue becomes thinner. Eventually, the pressure raises the temperature to such a point that complete decomposition of PAM occurs and the sample tube appears clean, suggesting that the combustion front temperature at 10 MPa is above 400 °C.

The significant decrease in the burning rate of the gelled mixture at pressures below 20 MPa (Fig. 3-1) can be explained based on the aforementioned observations of bubbling in the liquid/gas interface region and its accelerating effect on the burning rate [8]. The higher viscosity and likely higher surface tension of the gelled propellant inhibit the growth of bubbles, decreasing the

turbulence at the liquid-gas interface, suppressing hydrodynamic instability, and decreasing the burning rate. Gelling may also affect the critical point of the mixture, which may explain the absence of the jumps in the burning rate, observed in the ungelled propellants.

The obtained information on the combustion of gelled HAN/methanol/water propellants is important for high-pressure propulsion applications. Indeed, the use of the ungelled propellants at pressures higher than 12 MPa is problematic because of the significant burn rate fluctuations. Gelling results in a single pressure regime with a pressure exponent of 1.15, which, though higher than 1, is relatively low. It is also possible that an increased concentration of PAM would lower the pressure exponent.

3.3.2 Thermoanalytical experiments

Figures 3-3 and 3-4 show typical DSC and TGA curves, obtained at atmospheric pressure for the aqueous HAN solution and the propellant mixtures (both ungelled and gelled). The most prominent effect of the gellant here is the suppression of the sharp exothermic peak during HAN decomposition. This peak, seen in the DSC curve for the 82.4 wt% HAN sample, corresponds to a near vertical slope in the TGA curve. Gelling has smoothed out both the sharp exotherm in the DSC and the near-vertical slope section in the TGA. The endotherms in the DSC curves of the propellant mixtures are explained by vaporization of methanol (part of which could remain bonded at these temperatures), the formed HNO_3, and possibly other species.

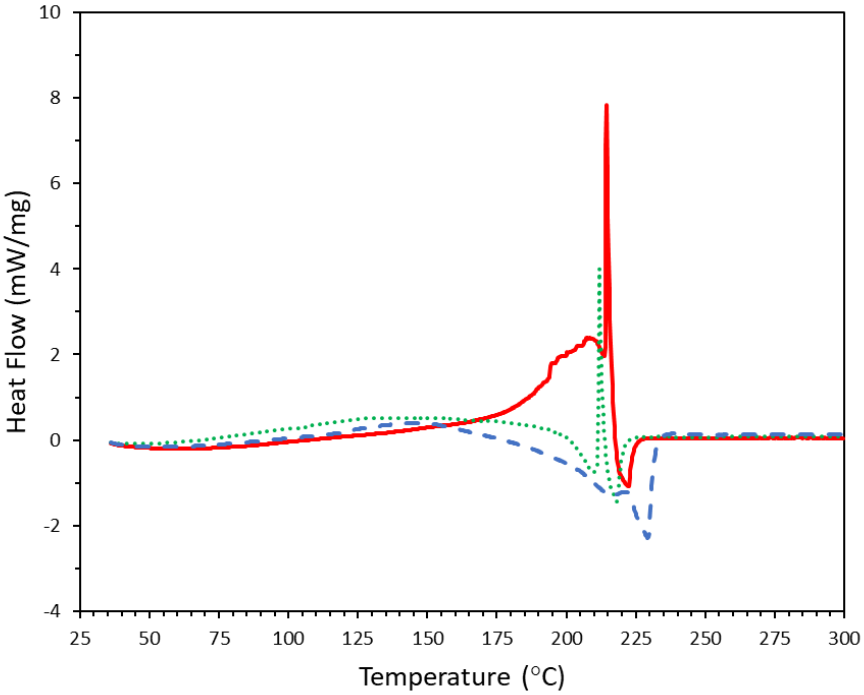

Fig. 3-3. DSC curves of 82.4 wt% HAN aqueous solution (solid red), ungelled propellant mixture (dotted green), and gelled propellant mixture (dashed blue).

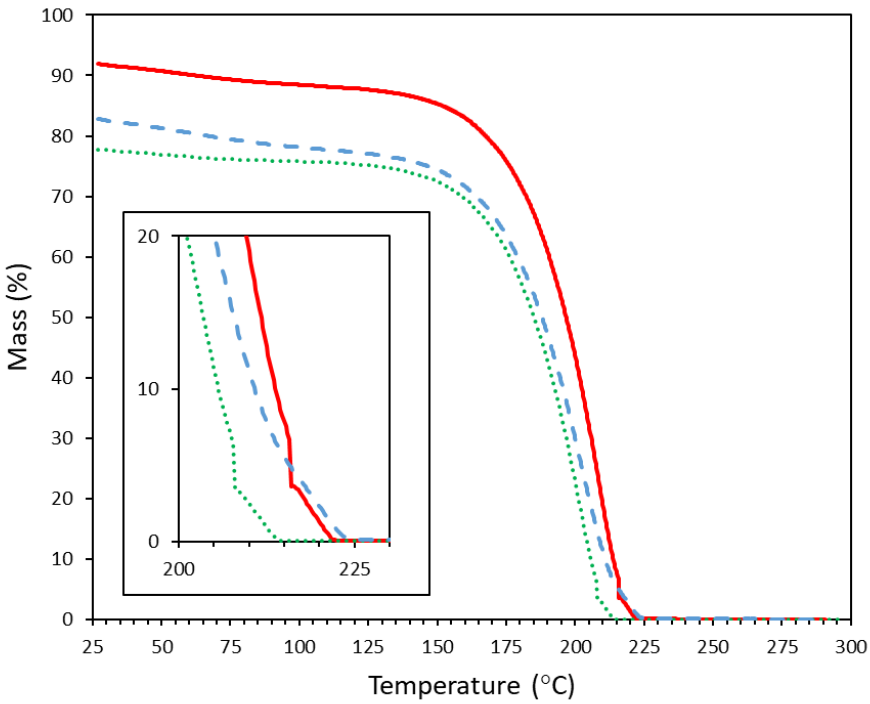

Fig. 3-4. TGA curves of 82.4 wt% HAN aqueous solution (solid red), ungelled propellant mixture (dotted green), and gelled propellant mixture (dashed blue).

Note that the TGA curves have been normalized to zero in Fig. 3-4. In the case of the ungelled propellant, no residue remains in the crucible after the test. While a brown residue does remain following gelled propellant testing, this has proven to be of negligible mass, which is consistent with the low concentration of PAM in the initial mixture. This residue is expected as the maximum temperature in the heating program was 300 °C, below the temperature required for full PAM decomposition. The loss of mass prior to the start of the heating program at 25 °C is the result of partial water and methanol evaporation during the isothermal gas purge.

Mass spectrometry of the gases evolved during DSC at atmospheric pressure has shown similar results to those of previous thermoanalytical studies of HAN decomposition [27, 28]. As shown in Fig. 3-5, the most prominent peaks are at mass-to-charge ratios of 18, 30, 44, and 46, indicating H_2O, NO, N_2O/CO_2, and NO_2, as well as HNO_3. To clarify, the highest peaks of HNO_3 are at m/z = 46, 30, and 18 (in the order of decreasing intensity) [29], and the peak at m/z = 46 in the mass spectrum of HAN decomposition is proven to be created by both NO_2 product and NO_2^+ fragment of HNO_3 [27]. A significantly smaller peak at m/z = 31 is likely the result of methanol evaporation (the highest peak in the electron-ionization mass spectrum of methanol is for COH_3^+ ion [30]).This signal falls significantly during the isothermal phase prior to the heating program (not shown), indicating most of the methanol was lost during this time. Apparently, as suggested above, some amount of methanol remains bonded at high temperatures and evolves during the decomposition of HAN, contributing to the endotherms in the DSC curves (Fig. 3-3).

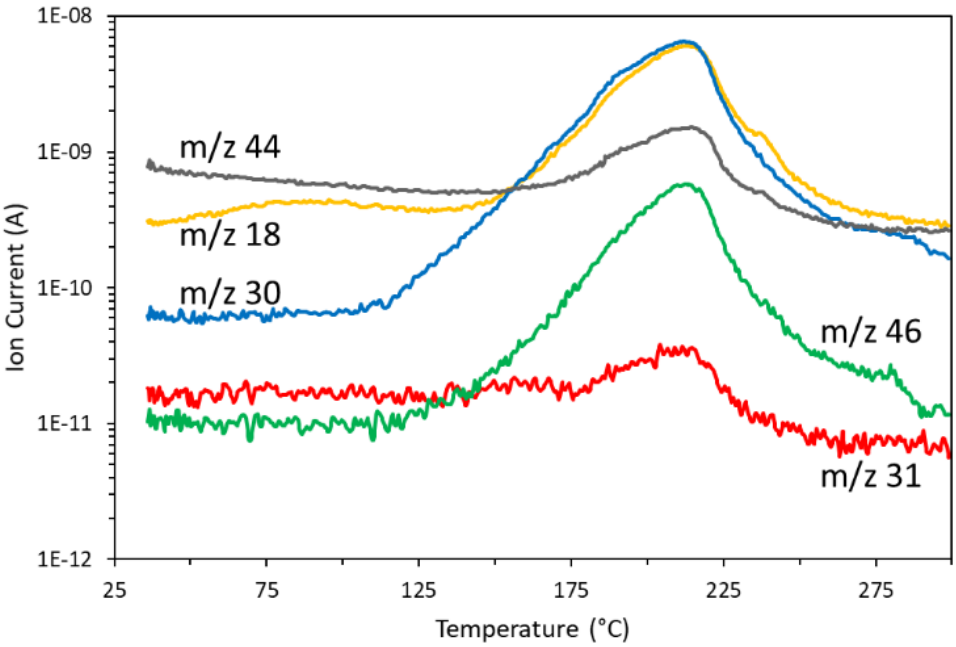

Fig. 3-5. Mass spectrometry results of gelled aqueous HAN/methanol mixture at atmospheric pressure.

Figure 3-6 shows typical high-pressure DSC curves for 82.4 wt% aqueous HAN solution, the aqueous HAN/methanol mixture, and the gelled aqueous HAN/methanol mixture at 5.1 MPa and 10 °C/min. It appears that regardless of the mixture composition, the decomposition of HAN remains the most significant event. Indeed, the addition of methanol or gellant did not make any noticeable change in the DSC curve. The shift of the peak for the gelled mixture toward a higher temperature in the curve shown in Fig. 6 is accidental, i.e., the scatter of data in several tests at identical parameters does not allow one to detect any systematic effect of gelling on the peak temperature.

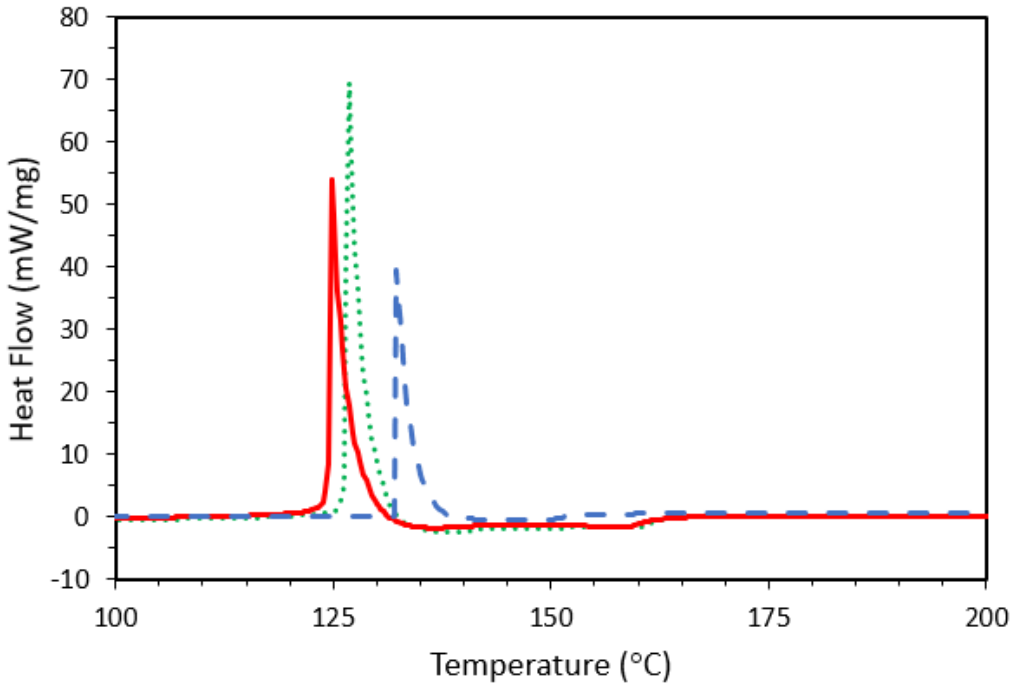

Fig. 3-6. HPDSC curves of 82.4 wt% HAN aqueous solution (solid red), liquid propellant mixture (dotted green), and gelled propellant mixture (dashed blue). Pressure: 5.1 MPa.

Further, in contrast with the DSC at atmospheric pressure (Fig. 3-3), gelling did not affect the shape of the exothermic peak. It is also seen that the exothermic peaks in the HPDSC curves are much higher than those in the atmospheric DSC tests. This provides further evidence that in the TGA and DSC at atmospheric pressure, a significant amount of important species, such as nitric acid formed at the initial step of the decomposition mechanism, is vaporized. In contrast, the high pressure combined with the absence of gas flow in the HPDSC tests suppress the vaporization.

Figure 3-7 shows the dependence of the DSC peak temperatures on pressure. It is seen that the composition of the sample mixture has little effect on the peak decomposition temperature. Some wider variation at the lower pressures is likely a result of experimental uncertainty, related to the vaporization of nitric acid, the saturated temperature of which strongly depends on pressure.

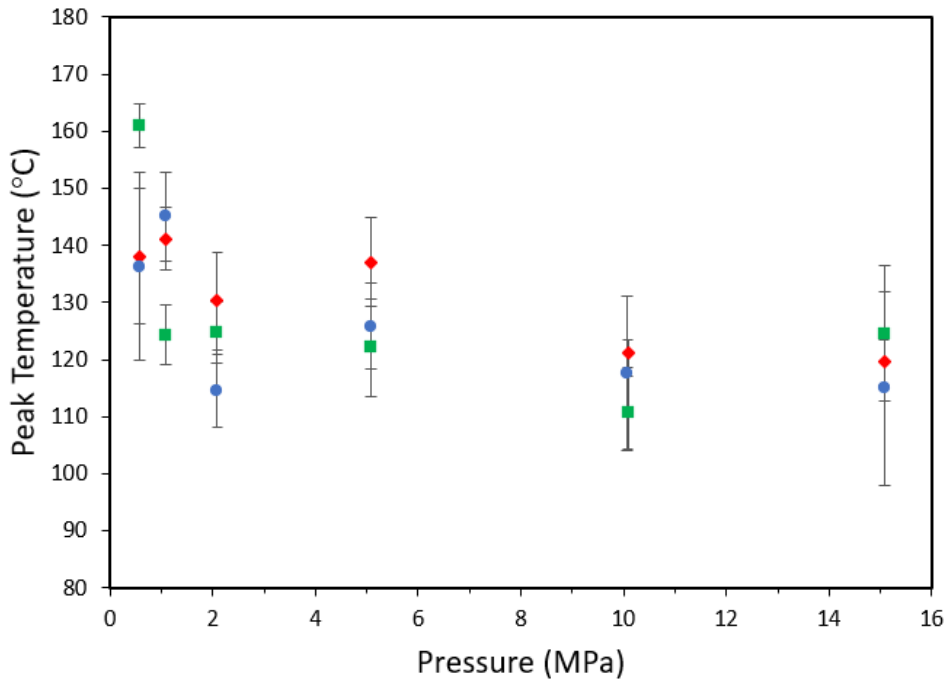

Fig. 3-7. HPDSC peak temperature of 82.4 wt% aqueous HAN (red diamonds), liquid propellant mixture (green squares), and gelled propellant mixture (blue circles).

Examining the TGA curves in Fig. 3-4, it is seen that when the period of rapid decomposition occurs, indicated by the near vertical slope in the curve, approximately 90% of the mass has already been lost. This period of rapid decomposition, as described above, corresponds to the sharp exothermic peak in the DSC curve. As a result, the sharp DSC peak apparently involves only roughly 10% of the original mass. Since the DSC heat flow is measured in mW/mg, and the original mass is used, the exothermicity of the reaction is much greater than Fig. 3-3 indicates. In addition, the cooling effect of the vaporization of HNO_3 and other species, which takes place in the atmospheric-pressure DSC, further decreases the peak intensity. In contrast, in the HPDSC, there is no gas flow, and the pressure raises the boiling points of condensed intermediate products such as HNO_3 and water. As a result, these volatiles remain in the sample and contribute to the reaction, resulting in the much higher exothermic peaks in Fig. 3-6.

t is also interesting to note that gelling the propellant did not result in much smaller, rounded peaks in the HPDSC (Fig. 3-6) as it did in the atmospheric DSC (Fig. 3-3). As noted above, the TGA and DSC at atmospheric pressure have shown that the exothermic peak occurs when most of the mass has been already lost. However, polyacrylamide decomposes at temperatures higher than those of HAN decomposition. Therefore, when the peak decomposition should take place, the PAM mass fraction in the remaining sample is much greater than the original 1 wt%, which in turn inhibits the reaction. By comparison, the sample in the HPDSC apparently remains near its original mass, the PAM fraction is not increased through loss of volatiles, and the exothermic peak remains of the same order as non-gelled samples.

The absence of influence of the gellant on the decomposition of HAN confirms that the observed strong effect of gelling on the combustion of the HAN/methanol/water propellant is related to hydrodynamics.

3.4. Conclusions

An aqueous HAN/methanol propellant mixture was gelled with 1 wt% polyacrylamide and ignited in a strand burner at pressures up to 30 MPa. The gellant suppressed fluctuations in the burning rate of the ungelled propellant associated with increasing pressure, leading to a single dependence with a pressure exponent of 1.15 ± 0.05 over the pressure range 4 – 30 MPa. The observed effect of gelling on the burning rate (the decrease) at pressures below 20 MPa may be associated with the suppression of bubble growth and hydrodynamic instability at the liquid-gas interface.

TGA and DSC of the aqueous HAN solution, the ungelled HAN/methanol mixture, and the gelled HAN/methanol mixture at atmospheric pressure indicated that a large part of the methanol evaporated prior to the decomposition of HAN, and the increased concentration of the gellant suppressed the exothermicity of the process by interfering with the HAN decomposition reactions. However, high-pressure DSC of these mixtures revealed that the decomposition of HAN is not chemically affected by the gellant or methanol (which could remain in the sample because of an increased boiling point). Thus, the thermoanalytical experiments confirmed that the effect of gelling on the combustion of HAN/methanol/water propellants is caused by hydrodynamic phenomena.

3.5. References

[1] R. L. Sackheim, R. K. Masse, Green propulsion advancement: Challenging the maturity of monopropellant hydrazine, *J. Propul. Power* **2014**, *30*, 265–276.

[2] S. R. Vosen, The burning rate of hydroxylammonium nitrate-based liquid propellants, *Proc. Combust. Inst.* **1988**, *22*, 1817–1825.

[3] S. R. Vosen, Hydroxylammonium nitrate-based liquid propellant combustion- interpretation of strand burner data and the laminar burning velocity, *Combust. Flame* **1990**, *82*, 376–388.

[4] Y.-P. Chang, E. Boyer, K. K. Kuo, Combustion behavior and flame structure of XM46 liquid propellant, *J. Propul. Power* **2001**, *17*, 800–808.

[5] Y.-P. Chang, K. K. Kuo, Assessment of combustion characteristics and mechanism of hydroxylammonium nitrate-based liquid monopropellant, *J. Propul. Power* **2002**, *18(5)*, 1076–1085.

[6] E. J. Wurcherer, S. Christofferson, B. Reed, Assessment of high performance HAN-monopropellants, *38th AIAA/ASME/SAE/ASEE Joint Propulsion Conference and Exhibit*, Huntsville, AL, USA, July 16-19, **2000**, p. 1–9.

[7] Y.-P. Chang, J. K. Kosten, B. Q. Zhang, K. K. Kuo, B. D. Reed, Combustion characteristics of energetic HAN/methanol-based monopropellants, *38th AIAA/ASME/SAE/ASEE Joint Propulsion Conference and Exhibit*¸ Indianapolis, IN, USA, **2002**, p. 1–14.

[8] T. Katsumi, H. Kodama, T. Matsuo, H. Ogawa, N. Tsuboi, K. Hori, Combustion characteristics of a hydroxylammonium nitrate based liquid propellant. Combustion mechanism and application to thrusters, *Combust. Explos. Shock Waves* **2009**, *45*, 442–453.

[9] K. W. McCown III, E. L. Petersen, Effects of methanol and fumed silica on linear burning rates of aqueous hydroxylammonium nitrate, *Int. J. Energ. Mater. Chem. Propul.* **2015**, *14*, 1–12.

[10] R. E. Ferguson, A. A. Esparza, E. Shafirovich, Combustion of aqueous HAN/methanol propellants at high pressures, *Proc. Combust. Inst.* **2021**, *38(2)*, 3295–3302.

[11] A. E. S. Nossier, A. Ceryone, A. Pasini, Review of state-of-the-art green monopropellants: For propulsion systems analysts and engineers, *Aerospace* **2021**, *8*, 1–21.

[12] B. Natan, S. Rahimi, The status of gelled propellants in year 2000, *Int. J. Energ. Mater. Chem. Propul.* **2002**, *5*, 172–194.

[13] M. B. Padwal, B. Natan, D. P. Mishra, Gel propellants, *Prog. Energ. Combust. Sci.* **2021**, *83*, 1–150.

[14] C. U. Kirchberger, M. Kurilov, S. Ricker, D. Freudenmann, Recent advances in gel propulsion technology at DLR Lampoldshausen, *12th International Symposium on Special Topics in Chemical Propulsion & Energetic Materials (12-ISICP)*, virtual, March 23-25, **2021**.

[15] W. F. McBratney, J. A. Vanderhoff, Burn-rate investigations of HAN-based candidate liquid propellants, Report No. ARL-TR-1927, Army Research Laboratory, Aberdeen Proving Ground, MD, USA, **1999**.

[16] J. L. Sabourin, R. A. Yetter, B. W. Asay, J. M. Lloyd, V. E. Sanders, G. A. Risha, S. F. Son, Effect of nano-aluminum and fumed silica particles on deflagration and detonation of nitromethane, *Propellants. Explos. Pyrotech.* **2009**, *34*, 385–393.

[17] B. N. Kondrikov, V. É. Annikov, V. Yu. Egorshev, L. T. De Luca, Burning of hydroxylammonium nitrate, *Combust. Explos. Shock Waves* **2000**, *36(1)*, 135–145.

[18] J. C. Thomas, G. D. Homan-Cruz, J. M. Stahl, E. L. Petersen, The effects of SiO_2 and TiO_2 on the two-phase burning behavior of aqueous HAN propellant, *Proc. Combust. Inst.* **2019**, *37*, 3159–3166.

[19] E. Shafirovich, V. Diakov, A. Varma, Combustion of novel chemical mixtures for hydrogen generation, *Combust. Flame* **2006**, *144*, 415–418.

[20] E. Shafirovich, V. Diakov, A. Varma, Combustion-assisted hydrolysis of sodium borohydride for hydrogen generation, *Int. J. Hydrogen Energy* **2007**, *32*, 207–211.

[21] G. A. Risha, J. L. Sabourin, V. Yang, R. A. Yetter, S. F. Son, B. C. Tappan, Combustion and conversion efficiency of nanoaluminum-water mixtures, *Combust. Sci. Technol.* **2008**, *180*, 2127–2142.

[22] Y. Sun, B. Zhu, H. Dang, H. Sun, Study on the flash pyrolysis of polyacrylamide: Accelerator of Al–H_2O-based propellants, *J. Mater. Sci.* **2011**, *46*, 4471–4478.

[23] D. A. Rodriguez, E. L. Dreizin, E. Shafirovich, Hydrogen generation from ammonia borane and water through combustion reactions with mechanically alloyed Al·Mg powder, *Combust. Flame* **2015**, *162*, 1498–1506.

[24] M. Tutas, M. Sağlam, M. Yüksel, Ç. Güler, Investigation of the thermal decomposition kinetics of polyacrylamide using a dynamic TG technique, *Thermochim. Acta* **1987**, *111*, 121–126.

[25] M.-H. Yang, The two-stage thermal degradation of polyacylamide, *Polymer Testing* **1998**, *17*, 191–198.

[26] A. Steudel, F. Friedrich, W. Lieske, W. Baille, D. König, R. Schuhmann, K. Emmerich, Simultaneous thermal analysis of cationic, nonionic, and anionic polyacrylamide, *Heliyon* **2019**, *5*, 1–6.

[27] T. Katsumi, R. Amrousse, Y. Niboshi, K. Hori, A Study on the combustion mechanism of hydroxylammonium nitrate, *Int. J. Energ. Mater. Chem. Propul.* **2015**, *14(4)*, 307–319.

[28] A. A. Esparza, R. E. Ferguson, A. Choudhuri, N. D. Love, E. Shafirovich, Thermoanalytical studies on the thermal and catalytic decomposition of hydroxylammonium nitrate solution, *Combust. Flame* **2018**, *193*, 417–423.

[29] R. A. Friedel, J. L. Shultz, A. G. Sharkey, Mass spectrum of nitric acid, *Anal. Chem.*, **1959**, *31(6)*, 1128.

[30] NIST Chemistry WebBook, NIST Standard Reference Database Number 69, Last update to data: 2021, https://doi.org/10.18434/T4D303.

4. Participants

Evgeny Shafirovich, Principal Investigator

Alan Esparza, Graduate Research Assistant

Robert Ferguson, Graduate Research Assistant

5. Products

5.1. Peer-reviewed Journal Articles

Ferguson, R.E., and Shafirovich, E., "Combustion of gelled HAN/methanol/water propellants," *Propellants, Explosives, Pyrotechnics* 46 (2021) 1672-1678.

Ferguson, R.E., Esparza, A.A., Chambreau, S.D., Vaghjiani, G.L., and Shafirovich, E., "Studies on the combustion of HAN/methanol/water propellants and decomposition of HAN and HEHN," *International Journal of Energetic Materials and Chemical Propulsion* 20 (2021) 21-31.

Ferguson, R.E., Esparza, A.A., and Shafirovich, E., "Combustion of aqueous HAN/methanol propellants at high pressures," *Proceedings of the Combustion Institute* 38 (2021) 3295-3302.

Esparza, A.A., Chambreau, S.D., Vaghjiani, G.L., and Shafirovich, E., "Two-stage decomposition of 2−hydroxyethylhydrazinium nitrate (HEHN)," *Combustion and Flame* 220 (2020) 1-6.

Thomas, A.E., Chambreau, S.D., Redeker, N.D., Esparza, A.A., Shafirovich, E., Ribbeck, T., Sprenger, J.A.P., Finze, M., and Vaghjiani, G.L., "Thermal decomposition and hypergolic reaction of a dicyanoborohydride ionic liquid," *The Journal of Physical Chemistry A* 124 (2020) 864-874.

5.2. Conference Presentations

Ferguson, R.E., Esparza, A.A., Chambreau, S.D., Vaghjiani, G.L., and Shafirovich, E., "Studies on the combustion of HAN/methanol/water propellants and decomposition of HAN and HEHN," 12th International Symposium on Special Topics in Chemical Propulsion and Energetic Materials (ISICP), March 23-25, 2021, Virtual.

Ferguson, R.E., Esparza, A.A., and Shafirovich, E., "Combustion of aqueous HAN/methanol propellants at high pressures," 38th International Symposium on Combustion, Jan. 24 – 29, 2021, Adelaide, Australia.

Ferguson, R.E., and Shafirovich, E., "Combustion of aqueous HAN/methanol propellants at high pressures," 50th JANNAF Combustion Subcommittee Meeting, Dec. 7-17, 2020, virtual.

Esparza, A.A., Shafirovich, E., Chambreau, S.D., and Vaghjiani, G.L., "Two-stage decomposition of 2−hydroxyethylhydrazinium nitrate (HEHN)," In-Space Chemical Propulsion Technical Interchange Meeting (TIM), Sep. 14-17, 2020, virtual.

Esparza, A.A., and Shafirovich, E., "Thermoanalytical study of hydroxylammonium nitrate decomposition at high pressures," AIAA Propulsion and Energy 2019 Forum, August 19-22, 2019, Indianapolis, IN, AIAA Paper 2019-4426.

Ferguson, R.E., Esparza, A.A., and Shafirovich, E., "Experimental study on the combustion mechanisms of HAN-based green monopropellants at high pressures," JANNAF 49th Combustion Subcommittee Meeting, June 3-7, 2019, Dayton, OH, Paper 2019-0001AD.

Esparza, A.A., Chambreau, S.D., Vaghjiani, G.L., and Shafirovich, E., "Thermoanalytical study on the decomposition kinetics of 2-hydroxylethyldrazinium nitrate," JANNAF 49th Combustion Subcommittee Meeting, June 3-7, 2019, Dayton, OH, Paper 2019-0001FK.

Thomas, A.E., Chambreau, S.D., Esparza, A.A., Shafirovich, E., and Vaghjiani, G.L., "Investigation of a hypergolic dicyanoborohydride-based ionic liquid," JANNAF 49th Combustion Subcommittee Meeting, June 3-7, 2019, Dayton, OH, Paper 2019-0001FL.

5.3. Dissertations and Theses

Ferguson, R.E., "Combustion of hydroxylammonium nitrate based monopropellants," PhD Dissertation, The University of Texas at El Paso, 2021.

Esparza, A.A., "Thermoanalytical studies on the decomposition of energetic ionic liquids," PhD Dissertation, The University of Texas at El Paso, 2020.

6. Awards

Ferguson, R.E., Esparza, A.A., and Shafirovich, E., "Combustion of aqueous HAN/methanol propellants at high pressures," Distinguished Paper Award in the Spray, Droplet and Supercritical Combustion Colloquium, 38th International Symposium on Combustion, Adelaide, Australia, 2021, https://www.combustioninstitute.org/news/2021-distinguished-paper-award-dpa-in-the-spray-droplet-and-supercritical-combustion-colloquium/